Title page

Title: **Simulations and observation of nonlinear internal waves on the continental shelf: Korteweg-de Vries and extended Korteweg-de Vries solutions**

First Author: Kieran O'Driscoll
Second Author: Murray Levine*

First Author address:
Kieran O'Driscoll
School of Natural & Built Environment
Queen's University Belfast
email: kieran.odriscoll@qub.ac.uk
Tel: +44 (0)28 9097 4204
Fax: +44 (0)28 9097 4278

*deceased

Simulations and observation of nonlinear internal waves on the continental shelf: Korteweg-de Vries and extended Korteweg-de Vries solutions

Kieran O'Driscoll[1], Murray Levine*

[1]Department of Civil Engineering, Queen's University Belfast, Belfast, BT9 1NN, Northern Ireland

*deceased

Correspondence to: Kieran O'Driscoll (kieran.odriscoll@qub.ac.uk)

Abstract. Numerical solutions of the Korteweg-de Vries (KdV) and extended Korteweg-de Vries (eKdV) equations are used to model the transformation of a sinusoidal internal tide as it propagates across the continental shelf. The ocean is idealized as being a two-layer fluid, justified by the fact that most of the oceanic internal wave signal is contained in the gravest mode. The model accounts for nonlinear and dispersive effects but neglects friction, rotation, and mean shear. The KdV model is run for a number of idealized stratifications and unique realistic topographies to study the role of the nonlinear and dispersive effects. In all model solutions the internal tide steepens forming a sharp front from which a packet of nonlinear solitary-like waves evolves. Comparisons between KdV and eKdV solutions is explored. The model results for realistic topography and stratification are compared with observations made at moorings off Massachusetts in the Middle Atlantic Bight. Some features of the observations compare well with the model. The leading face of the internal tide steepens to form a shock like front, while nonlinear high frequency waves evolve shortly after the appearance of the jump. Although not rank ordered, the wave of maximum amplitude is always close to the jump. Some features of the observations are not found in the model. Nonlinear waves can be very widely spaced and persist over a tidal period.

2

1. Introduction

Internal waves are present throughout earth's oceans wherever there is stratification, from the shallowest near-shore waters to the deepest seas. Internal waves are important to physical oceanographers because they transport momentum and energy, horizontally and vertically, through the ocean, e.g. Munk (1981), Gill (1982). They provide shear to turbulence which results in energy dissipation and vertical mixing, e.g. Holloway (1984), Sandstrom & Elliott (1984). Biological oceanographers are interested because the internal waves carry nutrients onto the continental shelf and into the euphotic zone, e.g. Shea & Broenkow (1988), Sandstrom & Elliott (1984), and Holloway et al. (1985). They are of interest to geological oceanographers because the waves produce sediment transport on the shelf, e.g. Cacchione & Drake (1986). Civil, hydraulic and ocean engineers are interested because the internal waves generate local tidal and residual currents, e.g. Willmott & Edwards (1987), which can cause scour on nearshore as well as offshore structures, e.g. Osborne et al. (1978). Large nonlinear IWs are also of interest to the navy because they cause large vertical displacements and large vertical velocities that may affect underwater operations.

This study is focused on the internal tide and subsequent evolution of nonlinear waves. Internal waves in the ocean span the frequency spectrum from the buoyancy frequency, N, to the inertial frequency, f. However, the internal, or baroclinic, tide accounts for a large fraction of the energy contained in these waves. The internal tide is generated by the interaction of barotropic tidal current with topography and not directly by the gravitational attraction of sun and moon. The properties and propagation of linear internal tide and waves have been treated in detail by many investigators, see, for example, Garrett & Munk (1979), or the monographs by Gill (1982), Lighthill (1978), or Apel (1987).

As the internal tide shoals, the nonlinear terms in the Navier-Stokes equations ~~become important.~~ ~~These~~can cause these tidal waves of finite amplitude ~~may~~to evolve into packets of high frequency nonlinear waves. The equations describing these waves are much more complex than the linear equations and few mathematical solutions have been found.

We are interested in nonlinear internal waves because they are a very energetic part of the signal in time series that we have observed on continental shelves and in the shallow ocean. We are guided by numerical solutions of Korteweg-de Vries (KdV) type equations that incorporate both weak nonlinear and weak dispersive effects.

The state of the art on the evolution of internal solitary waves across the continental shelf is reviewed in Grimshaw et al. (2010). Grimshaw et al. (2004) simulated the transformation of internal solitary waves across the North West shelf of Australia, the Malin shelf edge, the Arctic shelf; Holloway (1987) discussed the evolution of the internal tide in a two-layer ocean on the Australian North West Shelf. Our model simulations of the evolution of the internal tide across Middle Atlantic Bight topography are unique since these waves have never been modelled across such topography and stratifications, and the model results are compared with observations made at moorings off Massachusetts during the Coastal Mixing and Optics (CMO) Experiment. ~~For the model cases of~~Whereas most modelling studies regarding wave propagation over linear bottom sloping realistic topography~~, whereas most studies~~ have focused on the behaviour of a single soliton, this work is concerned with the development and evolution of a packet of solitary waves.

The goal of this paper is to study the observed variability in the evolution of the internal tide as it crosses the continental shelf resulting from different stratifications and varying topography.

4

In section 2, the model framework is presented, and model runs and results of simulations are discussed for cases of linearly sloping bottom topography and that at the site of the Coastal Mixing and Optics experiment (CMO). Model results are compared with data and observations collected at the CMO site in section 3. A summary and conclusions are presented in section 4.

5

2. Two-Layer Model

We are interested in modeling the evolution of the internal tide as it propagates shoreward from the shelf break. Since the greatest oceanic signal is the first internal mode, the stratification of the continental shelf/slope region is modeled as a two-layer fluid. This approximation greatly simplifies the
10 problem; the numerical scheme is much less complex for the two-layer case than the continuously stratified case, and the results are easier to interpret. Using this model configuration, we study the propagation of the internal tide over linear sloping and CMO topography. All cases have been run within the quadratic nonlinear framework of the KdV equation, and the results are compared with an extended form of it, the eKdV Eq.(1) model, written as

15
$$\eta_t + c\eta_x + (\alpha + \alpha_1\eta)\eta\eta_x + \beta\eta_{xxx} + \frac{c}{2Q}\frac{dQ}{dx}\eta = 0 \qquad\qquad 1$$

which reduces to the KdV equation when $\alpha_1 = 0$. The term in Q accounts for the horizontal variability of the ocean (see, e.g., Zhou & Grimshaw (1989), Pelinovsky et al. (1977) and Holloway et al. (1997)) and is given by $Q = \dfrac{Mc^3}{M_0 c_0^{\,3}}$ with $M = \dfrac{h_1 + h_2}{h_1 h_2}$ where h_1 and h_2 are upper and lower layer thicknesses, respectively. The coefficients of the KdV and eKdV equations are greatly simplified for a two-layer

5

fluid and are written (e.g. Ostrovsky & Stepanyants, 1989) $c = \sqrt{\dfrac{g\Delta\rho}{\rho}\dfrac{h_1 h_2}{h_1 + h_2}}$; $\alpha = \dfrac{3}{2}c\dfrac{h_1 - h_2}{h_1 h_2}$;

$\beta = c\dfrac{h_1 h_2}{6}$; $\alpha_1 = -\dfrac{3c}{8h_1^{\,2}h_2^{\,2}}\left(h_1^{\,2} + h_2^{\,2} + 6h_1 h_2\right)$.

For the KdV ~~Eq. (1)~~ and eKdV ~~Eq. (2)~~equations to be valid, the leading two terms must constitute the

$$\eta_t + c\eta_x + \alpha\eta\eta_x + \beta\eta_{xxx} = 0 \qquad\qquad 1$$

$$\eta_t + c\eta_x + (\alpha + \alpha_1\eta)\eta\eta_x + \beta\eta_{xxx} = 0 \qquad\qquad 2$$

primary balance. The nonlinear and dispersive terms can become important, but the assumptions leading to the KdV and eKdV equations are violated if either of the nonlinearity or dispersion terms approach the magnitude of the leading terms. Nonlinear ~~transformation~~steepening of the internal tide leads to the generation of a packet of short nonlinear waves which tend to become solitary-like in form as the dispersive term becomes important.

Note, the KdV equation is well known to be a suitable physical model for describing weakly nonlinear advective effects and linear dispersion in internal waves. It was originally developed by Benney (1966) and extended to second order by Lee & Beardsley (1974). The KdV ~~Eq. (1)~~ and eKdV Eq. (21) equations are derived following the procedure of Lee & Beardsley (1974) and the discussion by Lamb & Yan (1996). The two-layer KdV model approximation is discussed in Grimshaw et al. (2002), and justified since most of the energy in the ocean appears to be contained in the first mode anyway, see e.g. Alford & Zhao (2007). The coefficients of the KdV and eKdV equations are greatly simplified for a two-

layer fluid, e.g. Ostrovsky & Stepanyants (1989). The problem has been investigated for slowly varying topography and stratification by Grimshaw (1979) and Pelinovsky et al. (1977). An interesting reference is Lamb & Xiao (2014), who took a similar approach to ours, comparing predictions of the KdV and eKdV models, and also the RLW equation, with fully-nonlinear numerical simulations for two-layer stratification over selected topographies. See O'Driscoll (1999) for a full discussion of our experiments.

For all simulations the density difference between the two layers is chosen to be a constant: $g\Delta\rho/\rho = .014\,m/s^2$, a representative value for the Coastal Mixing and Optics (CMO) experiment (Levine & Boyd, 1999), for example at a mooring in the Middle Atlantic Bight located at 40.5°N, 70.5°W, and also in agreement with the stratification near the mooring location displayed in Barth et al. (1998).

2.1 The Korteweg de Vries (KdV) Model solutions

Using the KdV equation, we investigate ~~2~~two cases with a constant sloping bottom, one with a horizontal interface and one with a sloping interface, and finally make model runs with realistic topography at the CMO site.

For convenience in solving the equation, we avail of a transformation, utilized by Pelinovsky & Shavratsky (1976), of the space and time variables x and t to variables l and s, respectively, given by

$$s = \int_0^x \frac{dx}{c(x)} - t, \qquad l = x. \qquad\qquad \text{~~3~~2}$$

The transformed eKdV is then

$$\zeta_l + \frac{1}{c^2\sqrt{Q}}(\alpha + \alpha_1\zeta)\zeta\zeta_s + \frac{\beta}{c^4}\zeta_{sss} = 0 \qquad\qquad 4$$

~~where $\zeta = \eta\sqrt{Q(l)}$, $Q = \dfrac{Mc^3}{M_0 c_0{}^3}$, $M = \dfrac{h_1 + h_2}{h_1 h_2}$, and 0 subscripts represent initial values.~~

$$\zeta_l + \frac{1}{c^2\sqrt{Q}}(\alpha + \alpha_1\zeta)\zeta\zeta_s + \frac{\beta}{c^4}\zeta_{sss} = 0 \qquad\qquad 3$$

where $\zeta = \eta\sqrt{Q(l)}$ and Q is the same as for Eq.(1). The transformation scales time so that disturbances

5 traveling at the linear speed, c, remain at constant s. The system is often referred to as a slowness

coordinate system. Because ζ varies relatively slowly in l/c compared to s, terms such as $c\zeta_l$ are

neglected relative to ζ_s. The transformed KdV equation is the same as the transformed eKdV equation

with $\alpha_1 = 0$.

We employ the same finite difference scheme as Holloway et al. (1997) to solve the eKdV

10 equation Eq.(3) numerically. The finite difference scheme is a central difference method, (e.g. Lapidus

& Pinder, 1982), which was first developed for the KdV equation by Berezin (1987), and for the

variable coefficients KdV by Pelinovsky et al. (1994). See O'Driscoll (1999) for further details.

2.1.1 Constant Bottom Slope

15 The propagation of the internal tide along constant sloping topography was studied for cases of

constant upper layer thickness (Case A) and sloping interface (Case B), both of which are possible on

continental shelves. We chose the starting layer thickness at $l = 0$ ~~h1 =~~ to be $h_1 = 50m$ and ~~h2 =~~ $h_2 =$

150m, with a bottom slope of $1/1000$ so that total depth decreases from 200 to 0 m over a distance of 200 km.~~——~~ Note $\alpha_1 = 0$ for experiments discussed in section 2.1.

We first investigate the case of constant sloping bottom with ~~constant~~fixed upper layer thickness ($h_1 = 50m$. Case A). The value of c decreases in shallow water, while $\alpha \to 0$ as $h_2 \to$~~h_1~~ h_1 at a water depth of 100 m (Fig. 1a). Seaward of this depth where $h_2 > h_1$, $\alpha < 0$ and solitary waves are waves of depression, whereas shoreward of this depth ($h_2 < h_1$,), $\alpha > 0$ and solitary waves exist as waves of elevation only. $\beta \to 0$ as the product $h_2 h_1 \to 0$. As the magnitude of α is initially relatively large we expect the sinusoidal internal tide to transform rapidly resulting in the formation of several nonlinear waves. Since $\alpha \to 0$, these waves may not be so nonlinear as to violate the weakly nonlinear constraint on the KdV model. However, because the value of α rapidly increases for l~~>~~ > 100km, we expect the waves of elevation to become highly nonlinear thereby possibly violating the weakly nonlinear condition.

Figs. 1b and c show the internal tide signal for Case A at ~~different values of~~increasing l and ~~also~~ ~~at different water depths.~~decreasing depth. The internal tide steepens ~~and~~from a sinusoid at the open boundary, rapidly ~~becomes~~becoming nonlinear, resulting in the generation of a shock-like front and subsequent undulations by l~~≈~~ $\approx 50km$. Shoaling further, the internal tide becomes more nonlinear with the oscillations starting to resemble solitary waves by $l = 70km$. However, the waves never develop into mature internal solitary waves since the magnitude of α continually decreases. By $l = 90\ km$ the waves resemble a symmetric, dispersive packet~~, as further evidenced by~~ .~~Fig. 2a.~~ Initially the relatively large magnitude of α resulted in the rapid steepening of the internal tide. However, as ~~the value of~~ ~~$\alpha \to$~~$\alpha \to 0$ the nonlinear waves are prevented from developing into solitary waves, since higher order terms (neglected in the KdV) become of order α or larger and thus cannot be ignored, thereby rendering

9

Formatted: Body Text Indent 2, Line spacing: single

the KdV model invalid in this neighborhood. At $l = 100 km$ the packet certainly looks symmetrical about a horizontal axis, that is to say the waves are neither polarized as waves of depression nor elevation, since KdV solitary waves cannot exist when $\alpha = 0$. At $115 km$ the waves have switched polarity; they have become waves of elevation, a result of α having become positive. This transition is seen in Fig.~~2b~~2 where the leading waves are compared with sech^2 solitary form. Beyond $100 km$ the waves rapidly approach solitary waves of elevation since α becomes large quickly.

As the internal tide propagates into shallow water the ~~leading face~~front of the wave trough steepens but the decreasing magnitude of α causes this steepening to slow down and there is virtually no change in wave slope steepness between 70 and 90 km. The rate of change of the slope of the leading face of the trough changes sign when α becomes positive and the slope ~~steepens~~decreases rapidly, while the back face of the internal tide slackens. Fig.~~The steepening of the leading wave will lead to the formation of a second shock-like front (or a "reverse hydraulic jump" as has been described by Holloway et al., 1997). Fig.~ 1c gives a clear picture of the wave speed: the leading solitary-type wave initially travels with speed very slightly greater than c but becomes slower than c when l ~~~ 90km. The second solitary-type wave also has initial speed greater than c but becomes slower than c at l ~ 80km. All of the other waves travel with phase speed less than c. For l > 100km all waves travel with speed less than c, the reason becomes clear upon examination of Fig. 2a which plots the difference between the magnitudes of the nonlinear and dispersive terms~~ ~ $90 km$.

The leading waves are slightly more nonlinear than dispersive when $l \approx 70\ km$ but become less so as l approaches $100\ km$. When $\alpha = 0$ ($l = 100 km$) the value of the nonlinear term is zero and the waves look like a dispersive packet. Since $\alpha > 0$ for $l > 100\ km$, the nonlinear term is again a factor

10

and the waves become a hybrid by $l = 115km$, interchanging back and forth across the length of the wave between being more nonlinear and dispersive. The waves travel slower than c since the magnitude of the dispersive term is slightly greater than the nonlinear term.

For Case B with constant sloping bottom and sloping upper layer, we also begin in $200m$ water with $h_1 = 50m$, $h_2 = 150m$. In this instance the bottom slope is again $1/1000$ and the interface slope is $1/4000$ such that both layers vanish simultaneously at $l = 200\ km$. KdV parameter values are shown in Fig. 3a. The magnitude of α increases from $l = 0$ all the way to the shallowest water, unlike Case A where α passes through zero, so we expect the internal tide to become nonlinear sooner than for Case A, and any solitary waves to remain as waves of depression. ~~We do, however, expect the waves to become physically unstable, leading to a Kelvin-Helmholtz instability (see e.g. Cushman-Roisin & Beckers 2011), a result of the increasing magnitude of the nonlinear parameter combined with the decreasing value of the dispersive parameter.~~ This combination of events will result in the weakly nonlinear, dispersive KdV becoming invalid at $l = 95\ km$. Fig. 3b is a plot of the internal tide for Case B at several values of l. The internal tide steepens rapidly and a shock-like wave, followed by undulations, has evolved from the transforming tide by $l = 40km$. The internal tide continues to steepen and several nonlinear waves have formed by $l = 55km$. These leading nonlinear waves mature into rank ordered solitary waves by $65km$, a feature observed out to $95km$. Grimshaw & Yuan (2016) have recently shown that the rank ordering is retained in shoaling waters as long as the waves do not encounter a critical point of polarity change on the waves of depression, i.e. $\alpha < 0$ always. This was not the case for Case A (above, Fig. 1, and CMO, below, Fig. 4). Fig. 3c shows that most of the solitary waves eventually travel with phase speed greater than c. The waves are more nonlinear than dispersive and the increasing value of the nonlinear parameter

11

combined with the diminishing value of the dispersive parameter leads to the model becoming numerically unstable (O'Driscoll 1999).

2.1.2 Realistic topography and stratification

5   The CMO site was located in the Middle Atlantic Bight. CTD profiles were made across the continental shelf from shallow water to beyond the continental slope. Boyd et al. (1997) have concluded that the internal tide at the site is primarily a first mode internal wave, further justifying our choice of a two-layer model. An upper layer thickness of $25\ m$ is a representative average value for the duration of the experiment (July and August 1996).

10   Fig. 4a shows KdV parameter values as a function of l. Though undulating, the bottom topography is similar to the constant sloping bottom cases. Recall that we chose an upper layer depth of 50 m for Case A, whereas here we have chosen $h_1 = 25$ m. α starts out negative with relatively large magnitude. The magnitude decreases, similar to Case A, changing sign as the bottom shoals and $h_1 > h_2$ when the value increases rapidly. Values of $\beta,\ c$ and the horizontal variability parameter, $Q,$ are similar to Case A. Figs.

15 4b and c show results for tidal forcing of amplitude 2 m at 180 m water depth. The internal tide evolves similarly to Case A. A shock-like front has formed on the ~~back face~~front of the internal tide <u>wave trough</u> at $l = 40km$. Several nonlinear waves have formed by $l = 60km$ (mooring location) with the leading $4 - 5$ waves appearing like solitary waves of depression and the trailing waves looking more like a dispersive packet. Several more waves have formed by $80km$ but the number of solitary-like waves

20 seems to have been reduced to the leading two waves. All of the trailing waves do appear as a dispersive packet since the magnitude of α has decreased. More waves continue to form but by $100\ km$ the packet

12

is neither a pack of waves of elevation nor depression, not unlike Case A. Beyond $l = 125km$, α becomes large, the waves reverse polarity and rapidly develop into mature solitary waves of elevation. The results show that the CMO case and Case A are similar, though more solitary waves have formed for the CMO case, due to the fact that at the CMO site the value of α is initially twice that of Case A. The internal tide becomes <u>numerically</u> unstable beyond $l = 130km$~~, a result of the increasing value of the nonlinearity parameter combined with the vanishing dispersion parameter~~. Fig. 4c is a plot of the evolution of the internal tide as it propagates over the continental shelf, increasing in l. The leading solitary-like waves initially travel with speed very slightly greater than c, as in Case A. The waves slow down to travel at speed c where $l \approx 90km$ and α is very small. Wave speed then becomes slightly slower than c but faster and more complicated than Case A, due to the undulating topography.

~~The difference in magnitudes of the nonlinear and dispersive terms, $\chi = \left|\frac{\alpha}{c^2}\eta\eta_s\right| - \left|\frac{\beta}{c^4}\eta_{sss}\right|$, is plotted in Fig. 5. The leading 2-3 three waves are initially more nonlinear than dispersive but the diminishing magnitude of α leads to the waves becoming more dispersive like and the waves begin to slow down. The negligible value of α between $l = 100 - 115\ km$ results in the waves acting very much like a dispersive packet and they travel with wave speed slightly less than c. The increasing value of α after it passes through zero, leads to the nonlinear term becoming almost the same order of magnitude as the dispersive term before the model becomes numerically unstable shortly beyond $l = 130\ km$.~~

2.2 The extended Korteweg - de Vries (eKdV) model

13

The model runs discussed in section 2.1 were also made with the eKdV equation. The ratio of the nonlinear parameters, $\frac{\alpha}{\alpha_1} = 4\frac{h_1 - h_2}{h_1 h_2 \left(h_1^2 + h_2^2 + 6 h_1 h_2\right)}$ (see e.g. Ostrovsky & Stepanyants, 1989) is the theoretical maximum amplitude for the solitary wave solution to the eKdV equation. The ratio of the quadratic to cubic nonlinear terms in this equation depends upon displacement height, η, and is given by

5   $\frac{\alpha}{\alpha_1 \eta}$.

For Case A the ratio $\frac{\alpha}{\alpha_1}$ passes through zero ($h_1 = h_2$) (Fig. S1) and we expect the cubic nonlinear term to be important. The results of this model run are shown in Fig. 6̶5. The internal tide evolves similar to the KdV case (Fig. 1b) with a shock-type wave followed by several nonlinear oscillations on the back face of the internal tide at $l = 50 km$. The internal tide in both frameworks look

10   similar at 70 km where several nonlinear waves of depression have been formed. The KdV solitary-like waves flip polarity at 100 km due solely to the fact that α changes sign there.

For the CMO case, comparison of KdV and eKdV results shows a more significant difference than for Case A. Fig. 7̶a̶6a-c show the KdV and eKdV model results for a $4m$ internal tide having propagated

15   60 km to a water depth of 69 m. The leading KdV model solitary wave (solid line) arrives at the CMO central mooring ~0.1 tidal period ahead of the leading eKdV model solitary wave (broken line). The KdV and eKdV models are so different at the CMO site when compared to Case A because the magnitude of α_1 is greater at the CMO site. Though the magnitude of α is less in Case A, the fact that the magnitude of α_l is so small when compared to α means the addition of the cubic nonlinear term does little to change

14

the KdV results. This is not true at the CMO site where the greater magnitude of α_l is the reason for the difference between the KdV and eKdV frameworks, particularly as the internal tide propagates into shallower water and the magnitude of the ratio $\frac{\alpha}{\alpha_1}$ is much greater for Case A, where h_1 and h_2 are, respectively, twice and less than that at the CMO site. Comparing the leading waves from the eKdV and

5   KdV solutions reveals a fundamental difference in wave form; the KdV waves are taller and thinner (Fig. 7c6c). Solitary type solutions to the KdV (sech^2) and to the eKdV (tanh, also known as '('table-top' waves with tanh type solutions, see O'Driscoll 1999 and references within) are fitted to the leading waves (Fig. 7d6d-e). The leading wave in the KdV model is very well approximated by a sech^2 wave. The lead wave in the eKdV model is neither well approximated by sech^2 or table-top wave, but appears to be a hybrid

10   between the two. Fits of sech^2 and table-top waves were made by subjectively choosing values of η_0 and υ, respectively, while using the value of KdV and eKdV parameters for $69m$ water depth. Note that the amplitude of the table-top wave is limited to $\frac{\alpha}{\alpha_1}$. Increasing υ only serves to make the waves wider once its value is close to one (see e.g. O'Driscoll 1999). Amplitude and width of the leading waves in the packet are also compared in Fig. 8a7a. The width is defined as the time it takes the wave to pass a fixed

15   point, as measured at 42% of the amplitude. Results from a range of different tidal amplitudes are also shown. For reference, the dotted lines represent sech^2 and table-top waves for the local values of parameters h_1, h_2, and $g\Delta\rho/\rho$. For KdV the leading wave of the $2m$ tide always has amplitude greater than the second and the amplitudes of subsequent waves decrease in a rank ordered fashion. The leading wave is slightly thicker than the trailing ones which are all approximately equal in width. For the eKdV the

20   leading wave has larger amplitude and is thicker than the trailing waves. For the KdV model with $4m$

15

amplitude tide all the waves fall on the same spot on the sech^2 curve. For the eKdV model with $4m$ amplitude tide, the waves appear on the 'thick' side of the sech^2 curve with the lead wave the most removed from the KdV theoretical curve. The same is true for amplitudes of 5m and 6m. The eKdV model waves appear to be evolving toward the theoretical eKdV 'tanh' curve. Note that the amplitude of many of these waves exceed the maximum amplitude of table-top/tanh waves of $9\ m$ as determined by the local parameters at the CMO site.

To learn more about the evolution of a sine wave to waves with sech^2 and table-top form, we ran the model with constant parameters (flat bottom) using values at the mooring site. The runs were made with initial tidal amplitudes of 1, 2 and 4 m in both KdV and eKdV frameworks and the width vs. amplitude for the first and second wave in each packet is plotted at various increments of l (Fig. 8b7b). The KdV waves grow in amplitude with approximately constant width before turning to hug the theoretical KdV line. They then decrease in amplitude while increasing slightly in thickness. Though the KdV model waves continue to evolve, most of them can be well approximated as being 'sech^2' waves after $\sim 100km$. For the eKdV case, the waves are initially close to the theoretical sech^2 KdV curve. The waves move slowly towards the theoretical eKdV tanh curve, ultimately decreasing in amplitude and increasing in thickness. The last points have been plotted after the internal tide has propagated $\sim 240km$. It appears that these waves are evolving toward table-top form, but mature over a relatively long distance. Also, the amplitudes of the waves are greater than the theoretical eKdV maximum but their magnitudes decrease as the tide evolves.

Another investigation to explore the evolution in the eKdV model (constant parameters) was made using an initial condition of a sech^2 wave, the solitary wave solution to the KdV equation. sech^2

16

amplitudes of 4m, 7m, 9m, and 13m (Fig. 8e7c) were chosen. The sech^2 waves are rapidly transformed to table-top waves, e.g. the 4 examples plotted reach the theoretical eKdV curve after the wave has propagated about 10 km. A solitary sech^2 wave evolves much more rapidly to table-top form (Fig. 8e7c), as opposed to when it is part of a packet of waves (Fig. 8b7b). The reason for this has not been thoroughly investigated, but provides caution for treating a packet as a group of non-interacting waves.

3. Observations of Nonlinear Internal Waves

The data to be presented and discussed was collected during the CMO, for location see Fig. 98. The CMO experimental field program was conducted to increase our understanding of the role of vertical mixing processes in determining the mid-shelf vertical structure of hydrographic and optical properties. The field program was conducted on a wide shelf so as to reduce the influences of shelf break and nearshore processes. The data we discuss was collected from the CMO Central Mooring in July and August 1996, a time when a strong thermocline is present as a result of large-scale surface heating, Boyd et al. (1997).

3.1 Observations during the Coastal Mixing and Optics Experiment

The Central Mooring of the CMO experiment was located at 40º 29.50' N 70º 30.46' W in water depth of 69 m. A total of 24 temperature recorders and 5 conductivity sensors were distributed along the mooring. Currents were measured at 14 depths from an ADCP placed a few metres above the bottom.

Boyd et al. (1997) have calculated the first mode internal wave amplitude from the velocity time series for the period 29 July to the 31 August 1996 (year day 210 - 245, Fig. 109 i)). The dominant barotropic tidal signal in the Middle Atlantic Bight is semi-diurnal, and is strongest over the period day

17

241-245 during spring tide (Fig. ~~11~~10). A semi-diurnal signal is apparent in the first mode record, particularly during the spring tide period. A spectrum of the first mode amplitude (Fig. ~~12~~11) shows energy peak at both low and high tidal frequencies. Much of the high frequency energy is due to bursts or pulses of high frequency nonlinear internal waves that occur for a short period during the semi-diurnal tidal cycle. These nonlinear internal waves propagate shoreward across the continental shelf to the south of Martha's Vineyard. The energy at high frequency is greater over the period day 241-245 during spring tides (Fig. ~~12~~11). There is a clear maximum in energy at 2 cpd over this period, and a significant amount of energy is also contained at 4 cpd. The energy rapidly drops for frequencies greater than 4 cpd but there is a significant increase in energy at $\sim$50 cpd and $\sim$90 cpd. To help interpret these observations, we compare them with the two-layer eKdV model using the CMO parameters. Since we do not know where the internal tide is generated or its amplitude, the model was run assuming a sinusoidal internal tide at distances of 24 km, 48 km and 60 km seaward of the mooring site. Three initial amplitudes of 2 m, 4 m and 6 m were used at each distance. Fig. ~~10~~9 iii) shows the internal tide as it appears at the CMO mooring site for these nine cases. In all instances, the leading face of the periodic sinusoidal wave slackens (or flattens) as the internal tide propagates shoreward. This is followed by a steepening of the back face which develops into a shock-like front. The shock-like front is followed by oscillations which subsequently evolve into a packet of solitary-like waves.

This same pattern can often be seen in the observed time series of the first internal mode. Fig. ~~13~~12 shows several individual jumps at the CMO mooring. Fig. ~~13~~12 i) (top left panel) shows first modes which best match the model results of Fig.~~10~~ 9 iii). Some features of the observations compare well with the model. The slackened leading face of the tide is always followed by a steep - almost shock like - front

18

followed by several highly nonlinear short period waves. Although not rank ordered, the largest amplitude wave in the observed packet is always at or near the jump. The model results show that the amplitude of the jump is greater for larger initial condition, and decreases with distance from the point of generation. Although nonlinear waves continue to evolve, their amplitudes decrease as they propagate shoreward

5   from their generation point, and they become 'thicker', i.e. they become more table-top like. Though the modelled waves have amplitudes less than the theoretical ~~tanh~~ limit for local eKdV parameters, they nonetheless fit the shape of several observed waves at the CMO site.

There are also features of the observations that are not found in the model. Fig. ~~13~~12 i) (top left)

10   (f) and (g) differ in that the packet that follows the shock-like front, persists until the end of the tidal period, and the waves are spread apart from each other. Fig. ~~13~~12 i) top left (c) shows two packets of solitary-like waves propagating past the mooring site over a tidal period. The leading slackened face is followed by a shock-like front and a packet of solitary waves. The trailing face then slackens to assume a slope similar to the leading face but a second shock-like front, followed by a packet of solitary waves,

15   passes before the end of the tidal period. This could be from a second internal tide front coming from another generation site, there can be overlapping semi-circles of internal wave fronts from multiple generation sites, see for example discussion in Apel et al. (1988). Another possible generation mechanism is the nonlinear evolution of inertia-gravity waves forming behind internal solitary waves due to rotation, see further in Grimshaw et al. (2014) and Lamb & Warn-Varnas (2015). It is also possible that multiple

20   packets form each tidal period, due to different generation mechanisms such as multiple tidal constituents or harmonics of a tidal components as found, for example, at the site of the Littoral Optics Experiment

where the 4th harmonic of the semi-diurnal tide was used to successfully simulate the evolution of the internal tide (O'Driscoll 1999).

Another common observation that is not found in the model results is a 'drop' in amplitude

5 before the jump that occurs at the beginning of the wave packet. Fig. ~~13~~ 12 i) (top left) (h) shows that the first internal mode drops between day 243.5 and 243.6 but the slackening slope is restored before the arrival of the jump and packet of solitary waves. Similar 'drops' also occur in Fig. ~~13~~ 12 i) (top left) (b) and (e) and ii) (top right) (a) and (i). Another phenomenon observed is that the slope of the leading face of the tide changes sign before the packet in several of the examples in Fig. ~~13~~ 12 ii) (top right~~-~~). In

10 Fig. ~~13~~ 12 ii) (top right) (h) the low frequency slope changes sign at day 236, and the solitary waves appear as usual ahead of the trailing, low frequency signal. The signal becomes even more complicated when both a 'drop' and low frequency slope change are present, e.g. Fig. ~~13~~ 12 ii) (top right) (d). In this case, the slope of the leading slackening low frequency signal changes sign at day 242.5 and is followed by a packet of four solitary waves. The low frequency signal is restored before the passage of a jump

15 followed by a packet of five large solitary waves. The trailing face retains the slope of the low frequency signal. Fig. ~~13~~ 12 iii) (bottom) shows a series of jumps which are more complex than those in the top panels, though they retain the basic structure of the model results over the tidal period.

To examine the details of the wave packets themselves, the width vs. amplitude was estimated for each wave from all events during the period day 210-245 (Fig. ~~14~~ 13). These waves are plotted along with

20 the leading two waves from six of the nine model runs shown in Fig. ~~10~~ 9 iii). Also shown are the theoretical relations for solitary waves for the eKdV and KdV equations using CMO site parameters. The

observed nonlinear waves vary greatly in amplitude and width, generally having amplitudes of $5 - 25$ metres, and widths of $200 - 600$ seconds. Larger amplitude observed waves are well approximated by model runs with large initial amplitude, particularly the $4m$ model. The $6m$ model run from $24km$ seaward of the CMO site is also a very good match for several of the observed waves. A large fraction of observed waves with amplitude less than $15m$, and particularly less than $10m$, are much 'thinner' than model waves with similar amplitudes. However, it seems reasonable to say that the observed waves are a good fit to the model waves.

While some features of the observations are reproduced in the model, there are many differences. The eKdV model used here is highly idealized. There are many effects that have not been considered, including bottom and internal friction, earth's rotation and mean shear. Given these limitations, we conclude that the observations are reasonably well matched by our model.

4. Summary and conclusions

Observations of highly nonlinear internal waves contained in the first mode time series on the mid-continental shelf and in current meter records in shallow water have led us to investigate the transformation of the shoaling internal tide. Observations were made in the mid-continental shelf at the site of the Coastal Mixing and Optics Experiment (CMO). An existing model based on generalized KdV and eKdV equations has been simplified for use in a two-layer ocean, which is representative of realistic stratification. The model accounts for weakly nonlinear and dispersive properties of the internal tide. Earth's rotation, internal dissipation, bottom friction, and internal shear are not included. The internal tide was forced with a periodic sinusoidal boundary condition and allowed to propagate shoreward.

21

The model was first run within a KdV framework with realistic continental shelf, constant sloping bottom with flat and sloping interface, and CMO shelf parameters. The internal tide steepens on its back face as it propagates shoreward, a direct result of the much greater magnitude of the nonlinear term in comparison with the dispersive term. Nonlinear waves evolve from the internal tide after the back face forms a shock-like front. The waves can appear as a rank ordered packet with the leading waves traveling fastest, since they are the most nonlinear. The leading waves of depression usually travel faster than the linear wave speed, c, and nearly fit solitary wave form for local KdV parameters ("sech^2"). Waves of elevation also develop into sech^2 waves.

The model runs made within the KdV framework were also made within the eKdV framework which includes a cubic nonlinearity term scaled by α_1. The results may or may not be similar, depending upon the ratio of the two nonlinear terms, $\dfrac{\alpha}{\alpha_1\eta}$. If this ratio is large (much greater than one) the cubic nonlinear term is not important and the KdV and eKdV results are similar. If the ratio is of order one or less the eKdV may evolve differently from the KdV. For the constant bottom slope simulations the model results were similar in both frameworks. However, there are some significant differences to the waves that cross the shelf using CMO parameters. The modeled leading waves at the CMO mooring site were much 'thicker' than sech^2 waves with local KdV parameters, but they had not quite developed into solitary wave solutions of the eKdV equation ('tanh' or (table-top waves).

To better understand the evolution of waves toward table-top form in an eKdV framework, without the complications of varying parameters, model runs were made using constant eKdV parameters representative of the CMO site. Upon formation, the leading waves of the packet are similar to sech^2 waves. The waves become 'thicker' and tend toward the table-top form upon further propagation, but never reach

22

the theoretical ~~tanh~~eKdV curve in our limited domain. To help understand why the evolution of waves from being close to sech^2 waves to being close to ~~tanh~~table-top waves was so slow, the internal tide was forced with a sech^2 wave. The evolving sech^2 rapidly moves to the theoretical ~~tanh~~eKdV curve for all amplitudes. We conclude that the interaction between the solitary like-waves in a packet slows them from evolving into exact solitary 'sech^2' or '~~tanh~~table-top' waves.

Model runs with varying initial amplitudes and generation regions were made to help interpret the observations made at the CMO site. Some features of the observations compare well with the model. The leading face of the internal tide steepens to form a shock like front. Nonlinear high frequency waves evolve shortly after the appearance of the jump. Although not rank ordered, the wave of maximum amplitude is always close to the jump. Some features of the observations are not found in the model. Nonlinear waves can be very widely spaced and persist over a tidal period. The amplitude of the observed waves often decreases before the arrival of the jump, while the leading face may change slope before the jump arrives.

Individual observed waves were examined and the details compared to model results. The observed nonlinear waves vary greatly in amplitude and width, generally having amplitudes of between 5 and 25 metres, and widths of between 200 and 600 seconds. Larger amplitude waves are well approximated by waves evolving from large amplitude model waves. A large fraction of smaller amplitude observed waves, particularly less than 10 m, are thinner than model waves of similar amplitude. We conclude that the observed waves are a good match to modeled waves given the highly idealized eKdV model used, and the fact that we have neglected friction, rotation and mean shear.

Author Contribution

Kieran O'Driscoll conducted this work out while a graduate student at the College of Oceanic &

23

Atmospheric Sciences, Oregon State University, in partial fulfillment of the degree of Master of Science. Murray Levine was the student's advisor.

10

15

References

Alford, M.H. and Zhao, Z.: Global patterns of low-mode internal-wave propagation. Part I: Energy and energy flux. J. Phys. Oc., 37, 1829-1848, 2007.

Apel, J.R.: Principles of ocean physics, International Geophysics Series, Volume 38, Academic Press, pp.
20 634, 1987.

Apel J.R., R.F. Gasparovic, D.R. and Thompson, B.L. Gotwols.: Signatures of surface wave/internal wave interactions: Experiment and theory." Dyns. Atms. Ocs., 12, 89-106, 1988.

Barth, J. A., Bogucki, D., Pierce, S. D., and Kosro, P. M.: Secondary circulation associated with a shelfbreak front. Geophys.l Res. Letts., 25, 2761-2764, ~~1988~~1998.

25 Benney, D.J.: Long nonlinear waves in fluid flows. J. Math. Phys., 45, 52 – 63, 1966.

Berezin, Yu. A.: Modeling Nonlinear Wave Processes. VNU Science Press, pp. 182, 1987.

Boyd, T., Levine, M.D., and Gard, S.R.: Mooring observations from the Mid-Atlantic Bight, Oregon State University, Data Report 97-2, pp. 226, 1997.

Cacchione, D.A. and Drake, D.A.: Nepheloid layers and internal waves over continental shelves and slopes, Geo-Marine Lett., 6, 147-152, 1986.

Cushman-Roisin, B. and Beckers, J-M.: Introduction to geophysical fluid dynamics: physical and numerical aspects. Vol. 101. Academic Press, 2011.

Garrett, C. and Munk, W.: Internal waves in the ocean, Ann. Rev. Fluid Mech., 11, 339-369, 1979.

Gill, A.E.: Atmosphere-Ocean Dynamics, Academic Press, Inc., pp.662, 1982.

Grimshaw, R.: Slowly varying solitary waves. I. Korteweg - de Vries equation. Proc. R. Soc., Lond., Ser. A, 368, 359-375, 1979.

Grimshaw, R. and Yuan, C.: The propagation of internal undular bores over variable topography. Physica D: Nonlinear Phenomena, 333, 200-207, 2016.

Grimshaw, R., Pelinovsky, D., Pelinovsky, E., and Slunyaev, A.: Generation of large-amplitude solitons in the extended Korteweg–de Vries equation. Chaos: An Interdisciplinary Journal of Nonlinear Science, 12, 1070-1076, 2002.

Grimshaw, R., Pelinovsky, E., Talipova, T., and Kurkin, A.: Simulation of the transformation of internal solitary waves on oceanic shelves. J. Phys. Oc., 34, 2774-2791, 2004.

Grimshaw, R., Pelinovsky, E., Talipova, T., and Kurkina, O.: Internal solitary waves: propagation, deformation and disintegration, Nonlinear Processes in Geophysics, 17, 633-649, 2010.

Grimshaw, R., Guo, C., Helfrich, K. and Vlasenko, V.: Combined effect of rotation and topography on shoaling oceanic internal solitary waves, J. Phys. Oc., 44, 1116-1132, 2014.

Holloway, P.E.: On the semidiurnal internal tide at a shelf-break region on the Australian North-West Shelf, J. Phys. Oc., 14, 1787-1799, 1984.

Holloway, P.E.: Internal hydraulic jumps and solitons at a shelf break region on the Australian North West Shelf. J. Geophys. Res. Oc., 92, 5405-5416, 1987.

Holloway, P.E., Humphries, S.E., Atkinson, M., and Imberger, J.: Mechanisms for nitrogen supply to the Australian North-West Shelf. Aust. J. Mar. Freshw. Res., 36, 753-764, 1985.

Formatted: Font: Times New Roman, Font color: Auto, Pattern: Clear

Holloway, P.E., Pelinovsky, E., Talipova, T., and Barnes, B.: A nonlinear model of internal tide transformation on the Australian North West Shelf. J. Phys. Oc., 27, 871-896, 1997.

Lamb, K.G. and Yan, L.: The evolution of internal wave undular bores: Comparisons of a fully nonlinear numerical model with weakly-nonlinear theory, J. Phys. Oc., 26, 2712 – 2734, 1996.

Lamb, K. G. and Warn-Varnas, A.: Two-dimensional numerical simulations of shoaling internal solitary waves at the ASIAEX site in the South China Sea, Nonlinear Processes in Geophysics, 22, 289-312, 2015.

Lamb, K.G. and Xiao, W.: Internal solitary waves shoaling onto a shelf: Comparisons of weakly-nonlinear and fully nonlinear models for hyperbolic-tangent stratifications, Ocean Model, 78, 17-34, 2014.

Lapidus, L. and Pinder, G.F.: Numerical solution of partial differential equations in science and engineering, John Wiley & Sons, Inc., pp. 677, 1982.

Lee, C. and Beardsley, R.C.: The generation of long nonlinear internal waves in a weakly stratified shear flow, J. Geophys. Res., 79, 453-462, 1974.

Levine, M. and Boyd, T.: Nonlinear internal wave observations on the continental shelf. In The 1998 WHOI/IOS/ONR Internal Solitary Wave Workshop: Contributed Papers, 1999.

Lighthill, J.: Waves in fluids, Cambridge University Press, pp. 504, 1978.

Munk, W.H.: Internal waves and small-scale processes. Evolution of Physical Oceanography (B.A. Warren & C. Wunsch, eds.), Chapter 9. MIT press, Cambridge Massachusetts, 1981.

O'Driscoll, K.T.A.: Nonlinear internal waves on the continental shelf. MS Thesis, College Oceanic and Atmospheric Sciences, Oregon State Univ., pp.125, 1999.

Osborne, A.R., Burch, T.L., and Scarlet, R.I.: The influence of internal waves on deep-water drilling. J. Pet. Technol., 30, 1497, 1978.

Ostrovsky, L. A. and Stepanyants, Y.A.: Do internal solitons exist in the ocean? Rev. Geophys., 27, 293 310, 1989.

Pelinovsky, E. and Shavratsky, S. Propagation of nonlinear internal waves in the inhomogeneous ocean, Izv. Atmos. Oceanic. Phys., 12, 41 – 44, 1976.

Pelinovsky, E., Shavratsky, S., and Raevsky, M.A.: The Korteweg de Vries equation for nonstationary internal waves in an inhomogeneous ocean, Izv. Atmos. Oceanic. Phys., 13, 373 – 276, 1977.

Sandstrom, H. and Elliott, J.A.: Internal tide and solitons on the Scotian shelf: a nutrient pump at work., J. Geophys. Res., 89, 6415-6426, 1984.

Shea, R.E., and Broenkow, W.W.: The role of internal tides in the nutrient enrichment of Monterey Bay, California, Estuarine, Coastal and Shelf Sci., 15, 57-66, 1982.
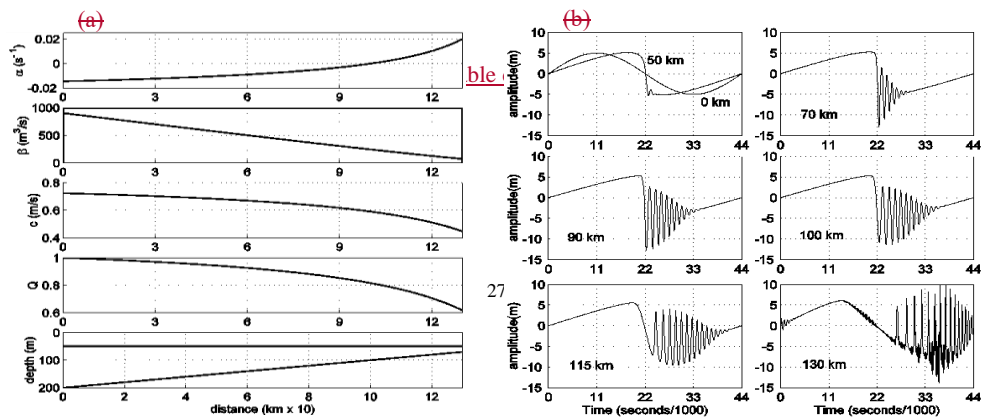
5 Willmott, A. and Edwards, P.D.: A numerical model for the generation of tidally forced nonlinear internal waves over topography, Cont. Shelf Res., 7, 457-484, 1987.
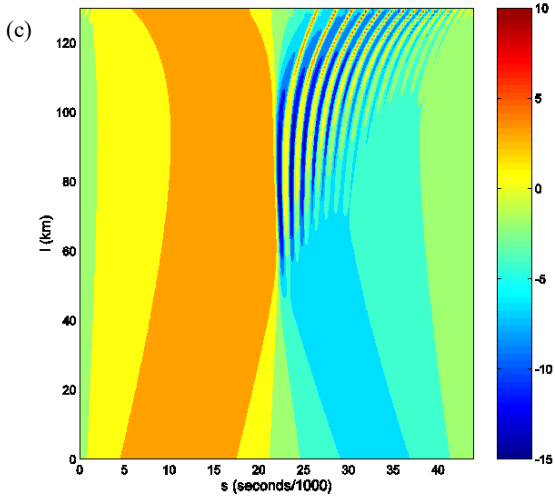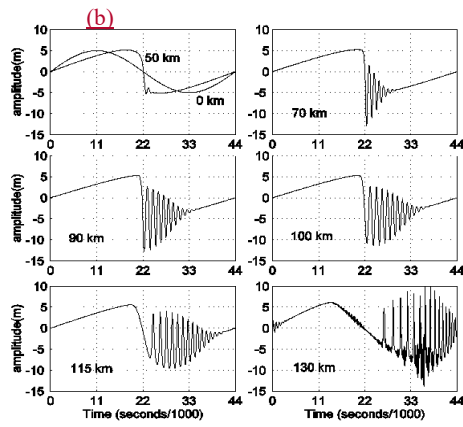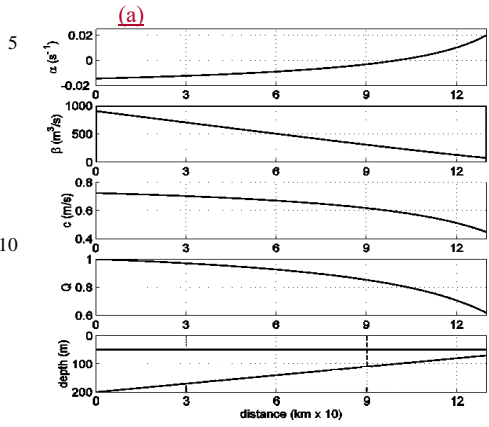
(a)

(b)

Formatted: Indent: Left: 2.54 cm, First line: 1.27 cm

(c)

Fig. 1. Case A (constant sloping bottom with level interface, $h_1 = 50$ m). KdV parameter values for quadratic nonlinear parameter, α, dispersion parameter, β, linear phase speed, c, horizontal variability factor, Q, and depth (**a**). Amplitude of the internal mode for two-layer fluid (**b**) at various distances from the boundary within KdV model framework and (**c**) as a function of distance l and time s within KdV model framework. The legend on the right corresponds to the amplitude of the waves (m).
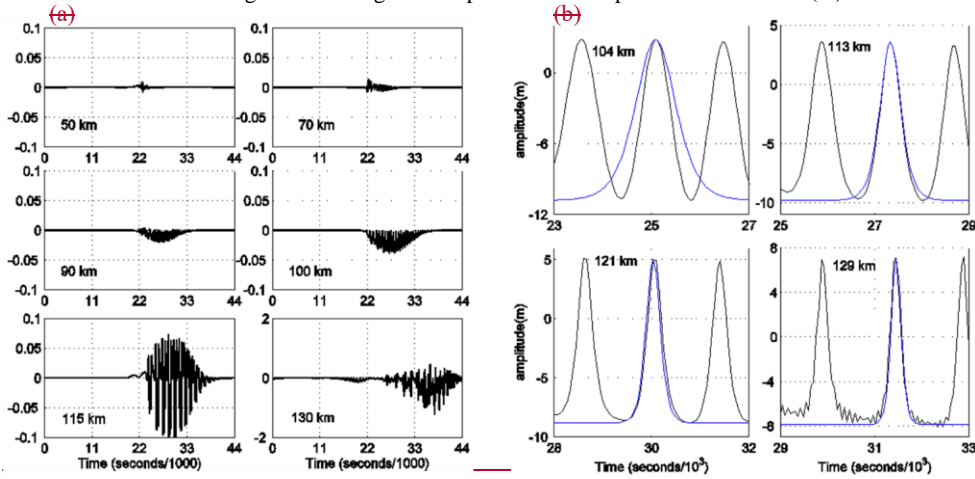
Fig. 2. Case A, (**a**) difference between the magnitudes of the nonlinear and dispersive terms at various distances from the boundary, and (**b**)
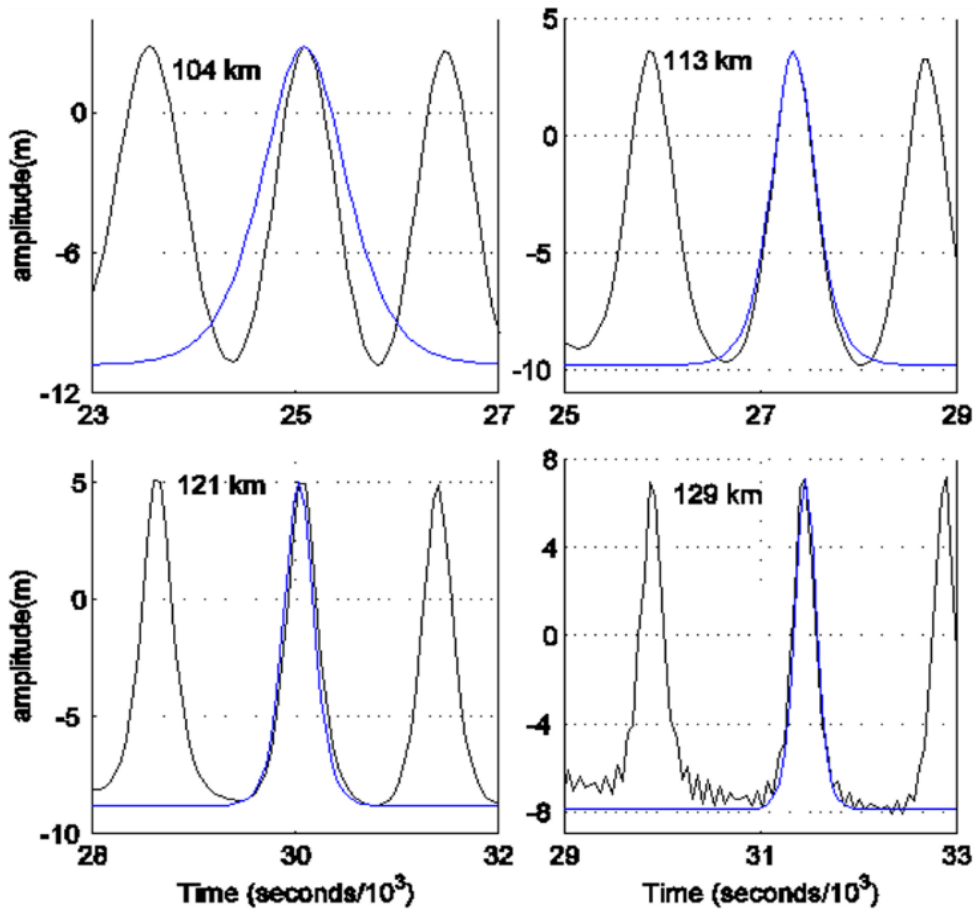
Fig. 2. Case A, leading waves of elevation (black line) at various distances $l > 100km$ from the boundary plotted with individual sech^2 waves (blue lines) within KdV model framework.

5

(a)

α (s^{-1})
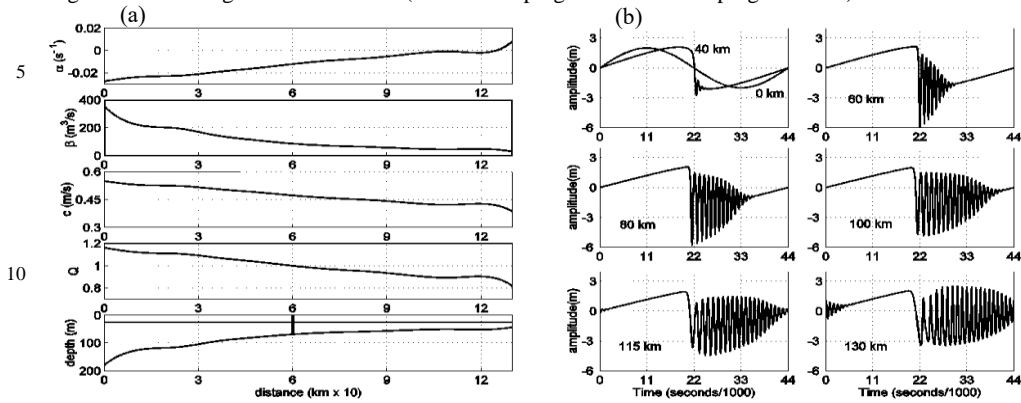
β (m^3/s)

c (m/s)

Q

depth (m)

distance (km x 10)

(b)

amplitude(m)

40 km   0 km

55km

amplitude(m)

65 km

75 km

amplitude(m)

85 km

95 km

Time (seconds/1000)   Time (seconds/1000)

(c)

31
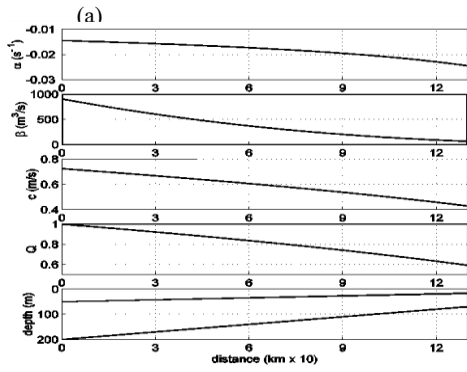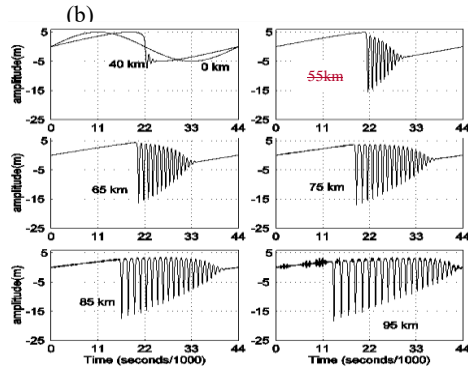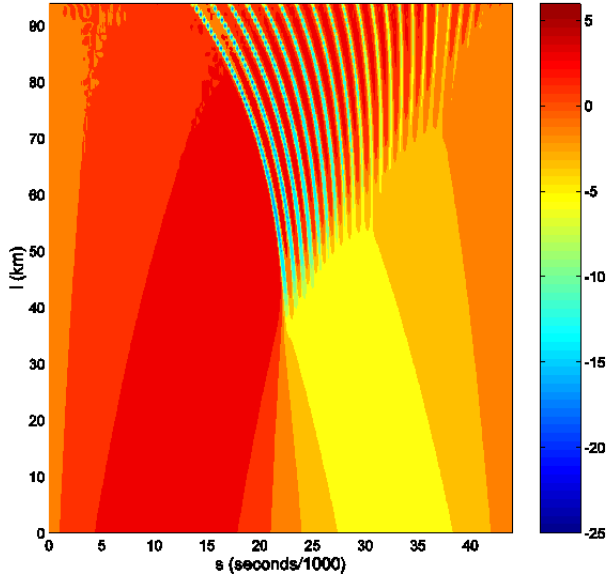
Fig. 3. Same as Fig. 1 but for Case B (constant sloping bottom with sloping interface).

(a)   (b)

5

10

(c)

32
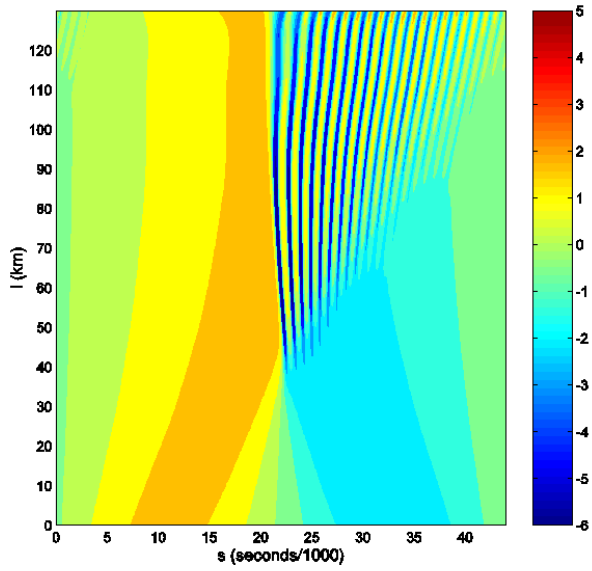
Fig. 4. Same as Fig. 1 but for CMO experiment site (with flat interface, $h_1 = 25\ m$).
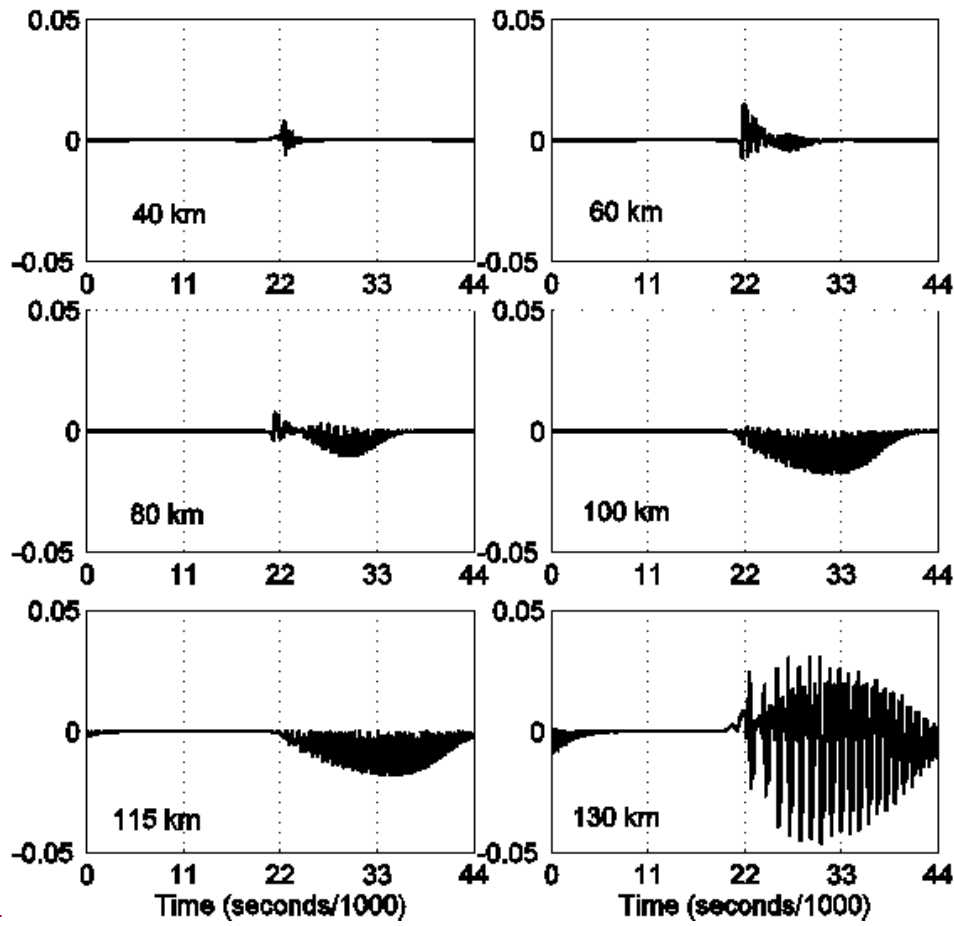
Fig. 5. CMO experiment site (with flat interface, $h_1 = 25\ m$) difference between the magnitudes of the nonlinear and dispersive terms at various distances from the boundary within KdV model framework.
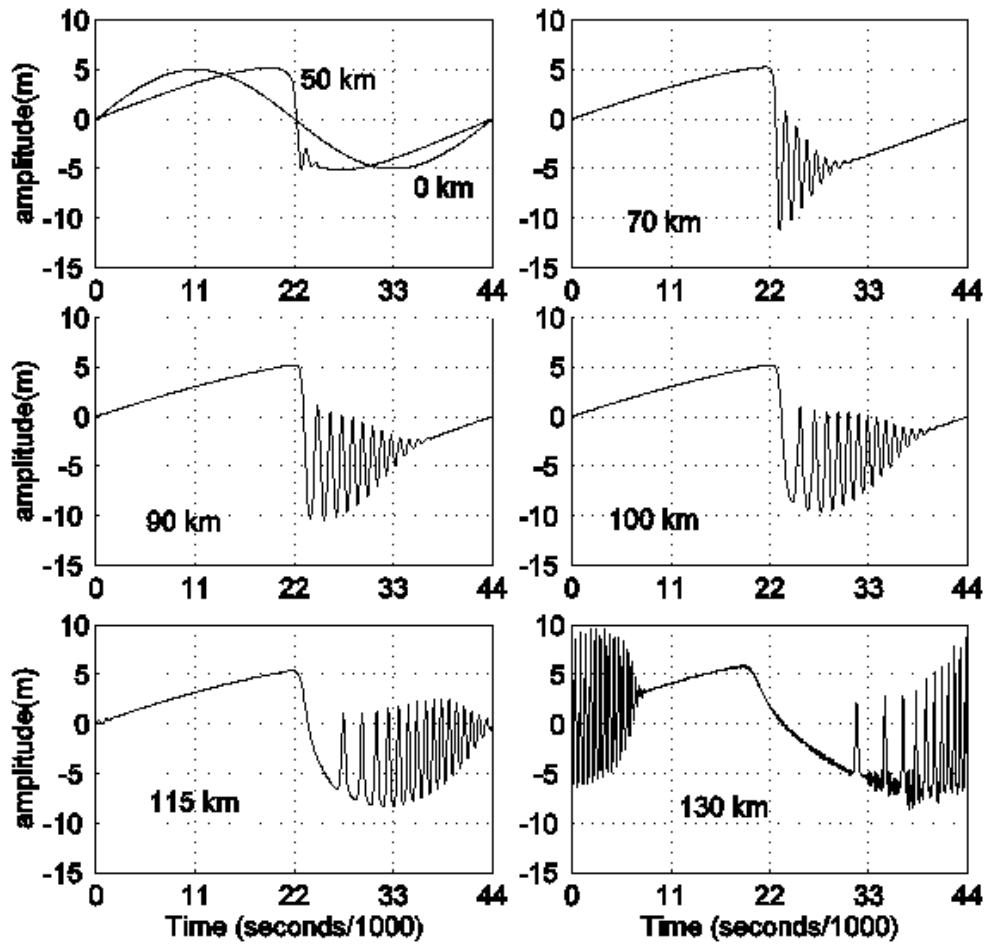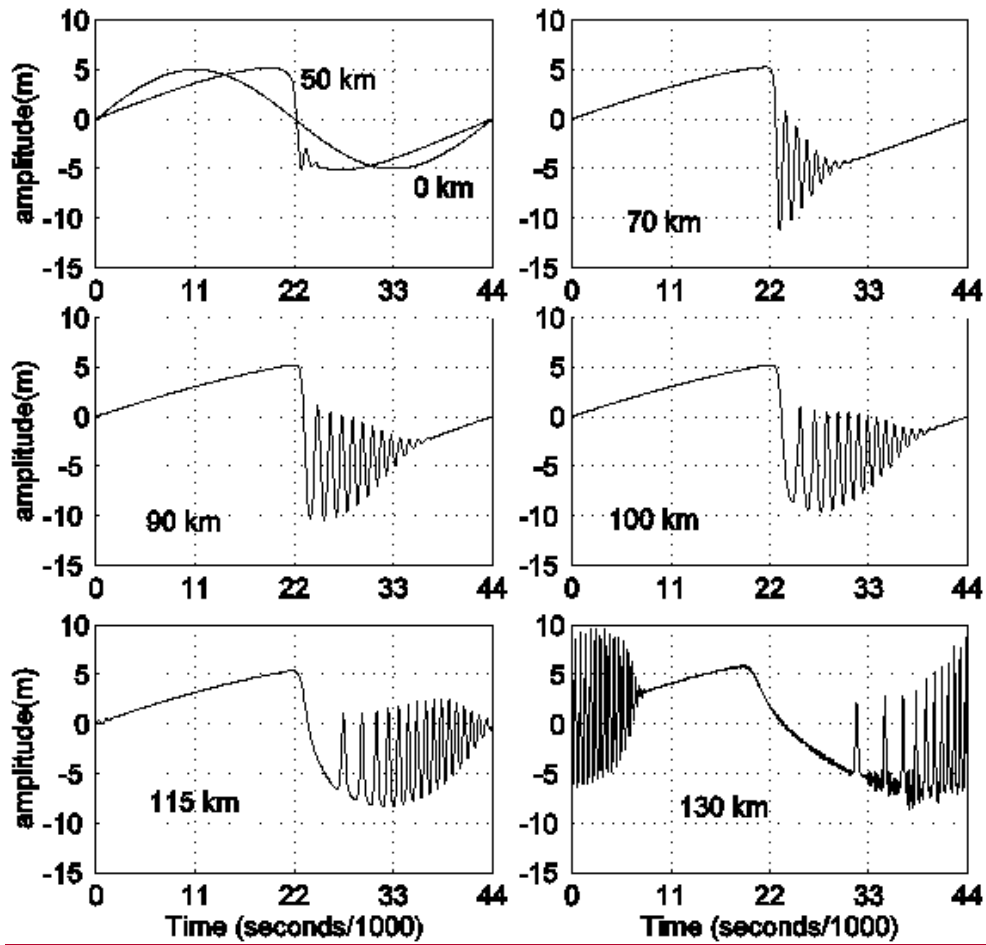
Fig. ————————————————————————————————— 6

Fig. 5. Case A (constant sloping bottom with flat interface, $h_1 = 50\ m$) amplitude of the internal mode for two-layer fluid at various distances from the boundary within eKdV model framework.
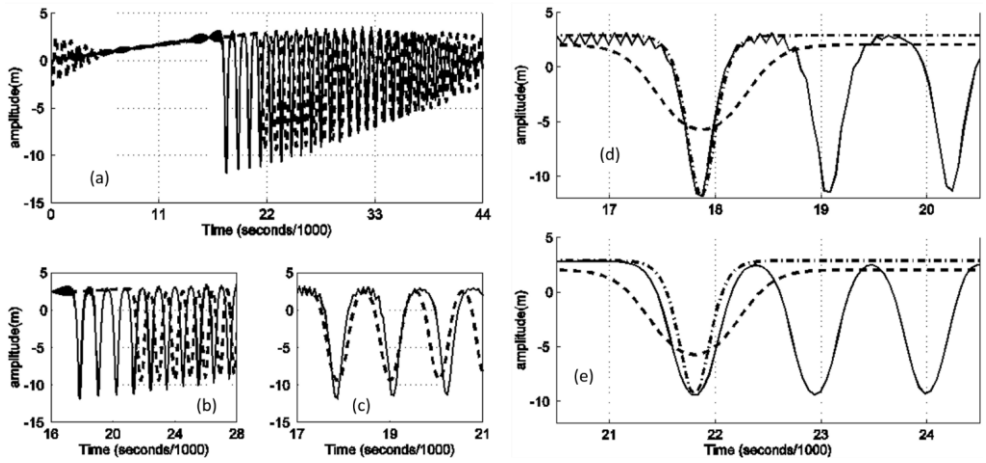
Fig. 76. CMO experiment site (realistic topography with level interface, ($h_1 = 25\ m$) amplitude of the internal mode for two-layer fluid at $60\ km$ in $69\ m$ depth water (CMO mooring site). **(a)** Comparison of KdV (solid line) and eKdV (broken line) solutions. **(b)** Close up of (a). **(c)** Leading KdV model waves (solid line) with superimposed eKdV model waves (broken line) shifted forward in time (s) so that the leading waves coincide. **(d)** and **(e).** The leading wave of depression (solid line) plotted with an individual sech² wave (dot-dash line) and with an individual ~~tanh~~table-top wave (dashed line) for KdV model (d), and eKdV model (e).
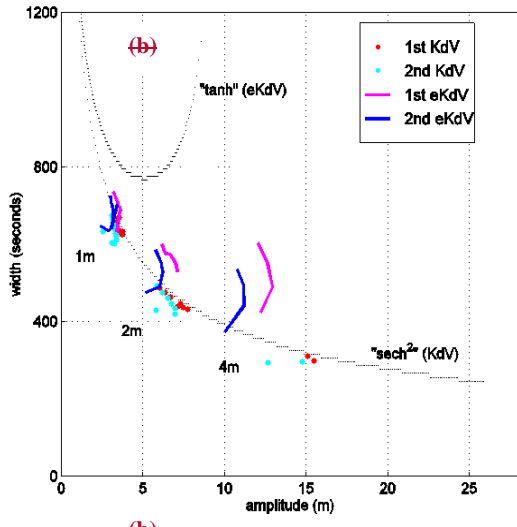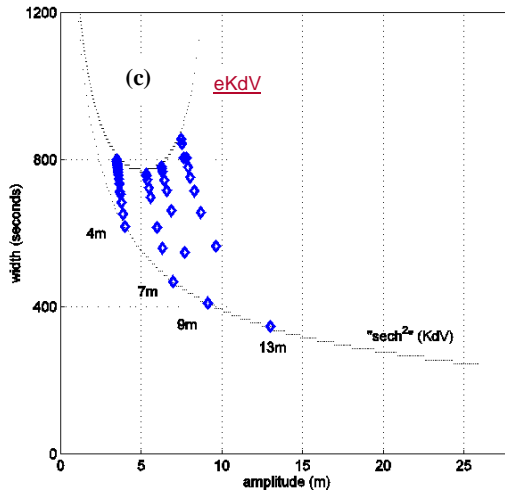
37
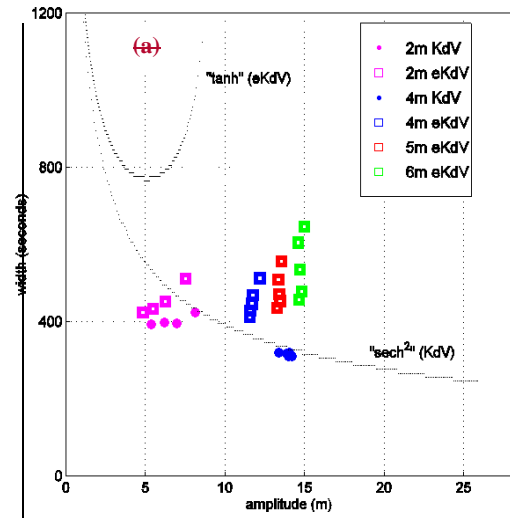
Fig. 8̶7̶. Width vs. amplitude of the leading waves of the KdV and eKdV solutions at the CMO mooring site ($h_1 = 25\ m, h_2 = 44m$) at $60\ km$ from the boundary in $69\ m$ depth water. Results for initial tidal amplitudes of 2, 4, 5, and 6 m are shown. The theoretical values for sech^2 and t̶a̶n̶h̶table-top waves using local parameters are also shown (dotted lines). The width is calculated at 42% of the total amplitude. **(b)** Evolution of the width vs. amplitude of the two leading waves of the KdV and eKdV solutions for flat bottom ($h_1 = 25$ m, $h_2 = 44$ m) with same parameters as at the CMO site. Results for initial tidal amplitudes of 1, 2, and 4 m are shown. A value is plotted every 10 km for the 1 m tide beginning at 160 km and the lines run from 160 km to 260 km. A value is plotted every 20 km for the 2 m tide beginning at 80 km and the lines run from 80 km to 200 km. A value is plotted every 20 km for the 4 m tide beginning at 40 km and the lines run from 40 km to 100 km. The theoretical width vs. amplitude for sech^2 and t̶a̶n̶h̶table-top waves is also shown (dotted lines), and the width is calculated at 42% of the total amplitude. **(c)** Evolution of the width vs. amplitude of four solitary sech^2 waves of the eKdV solutions for flat bottom ($h_1 = 25$ m, $h_2 = 44$ m) with same parameters as at the CMO site. Results are shown for sech^2 amplitudes of 4, 7, 9 and 13 m. A value is plotted every 1 km up to a maximum distance of 15 km. The theoretical width vs. amplitude for sech^2 and t̶a̶n̶h̶table-top waves is also shown (dotted lines). The width is calculated at 42% of the total amplitude.

39
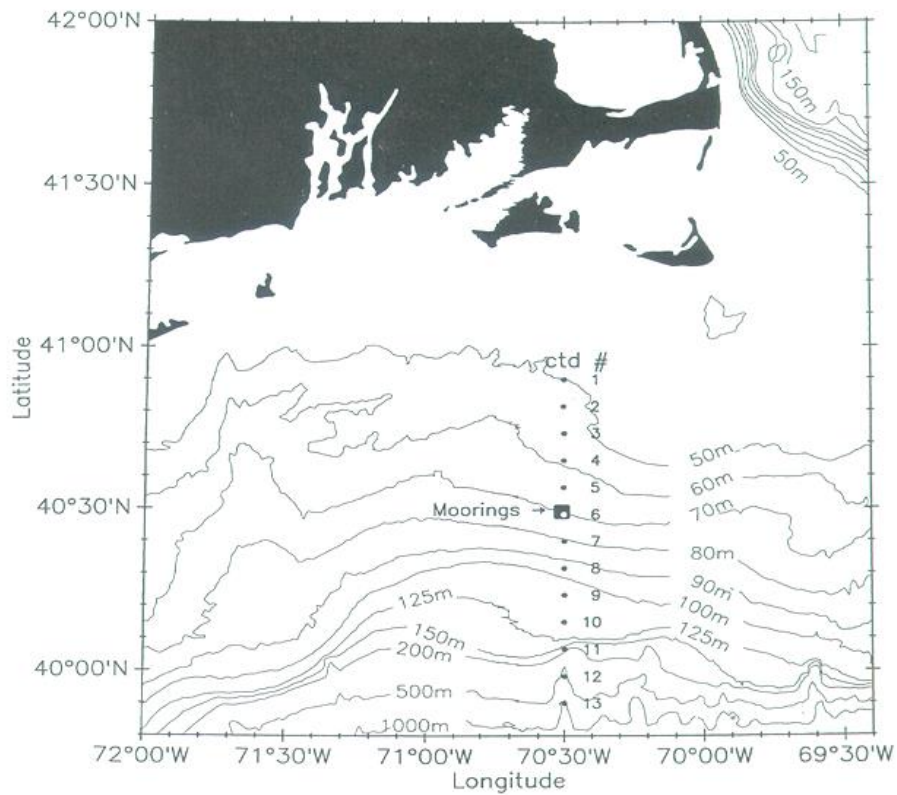
Fig. 98. Site of the Coastal Mixing & Optics experiment (left) located in the Middle Atlantic Bight to the south of Massachusetts. The data discussed was collected at the mooring marked 'CTD #6'.
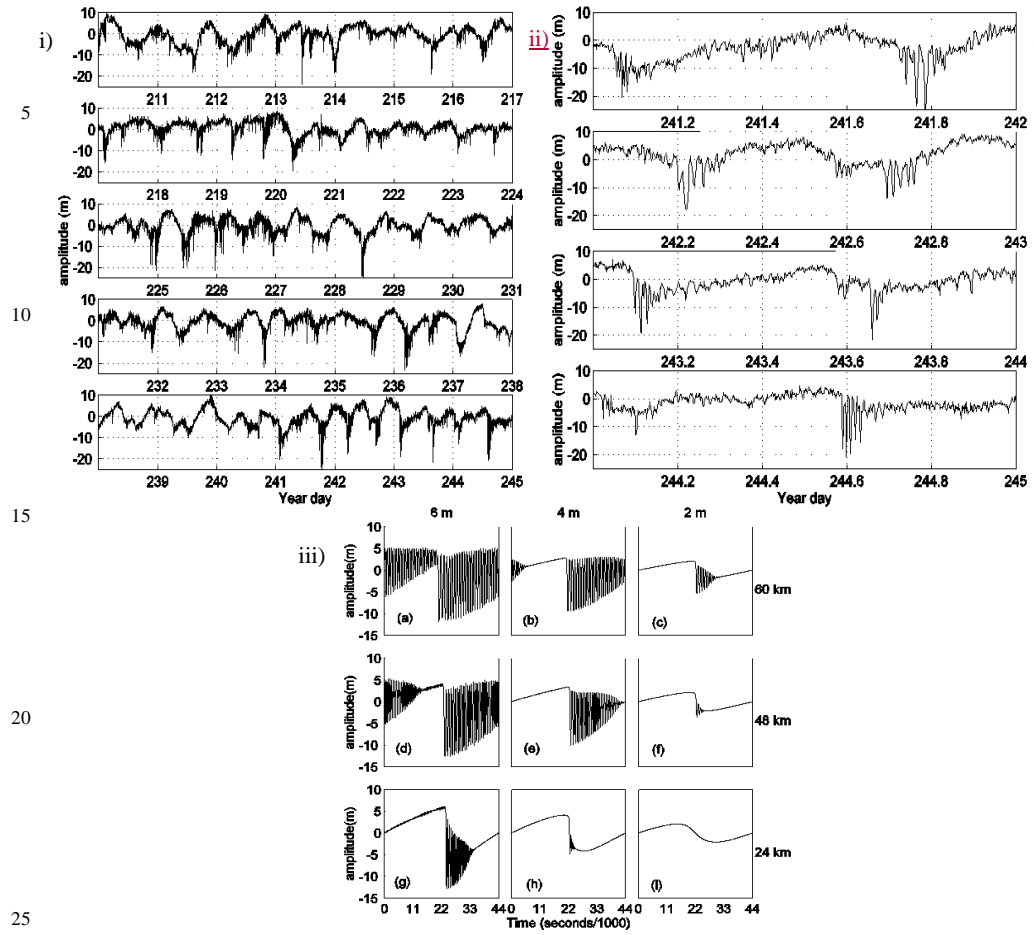
i)

ii)

iii)

Fig. 109. Top left, i), amplitude of the first internal mode calculated from the current meter record at the CMO mooring site over the period day 210-245 of 1996. Top right, ii), Same as i) except for the period day 241-245. Bottom, iii), three sinusoids of amplitude 2 m, 4 m and 6 m, respectively, and with tidal

41

period, as they appear at the CMO mooring site in the eKdV framework. The sinusoids have propagated shoreward from boundaries at 60 km, 48 km and 24 km offshore, respectively.

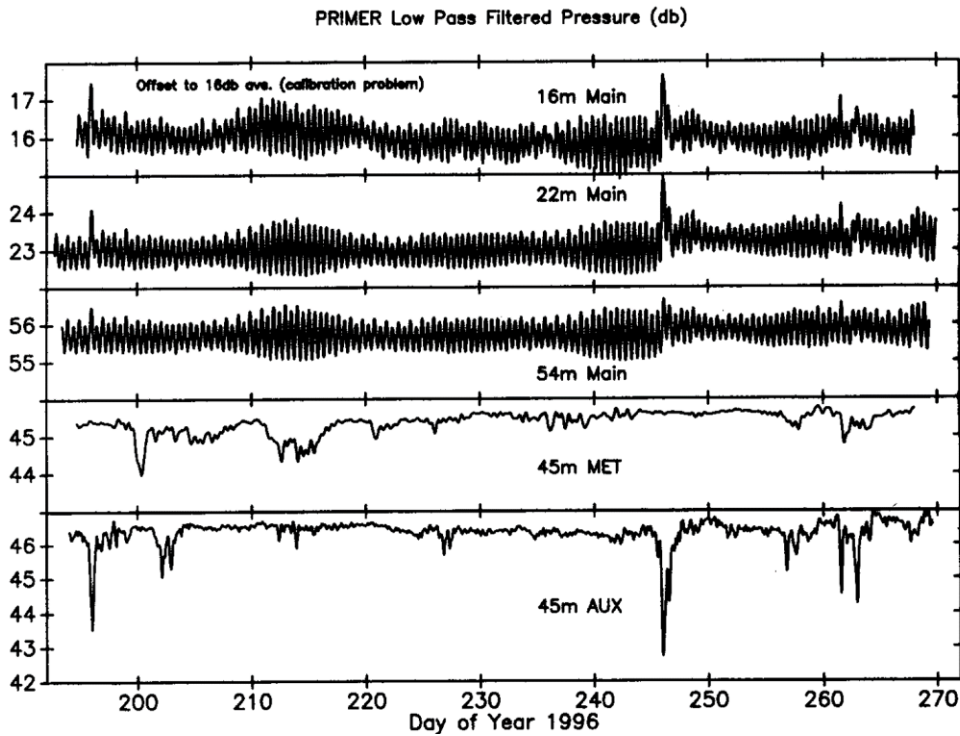PRIMER Low Pass Filtered Pressure (db)

Fig. 1110. Pressure (tidal) record at the CMO mooring site including for the period day 210 – 245 1996 (from Boyd et al., 1997).
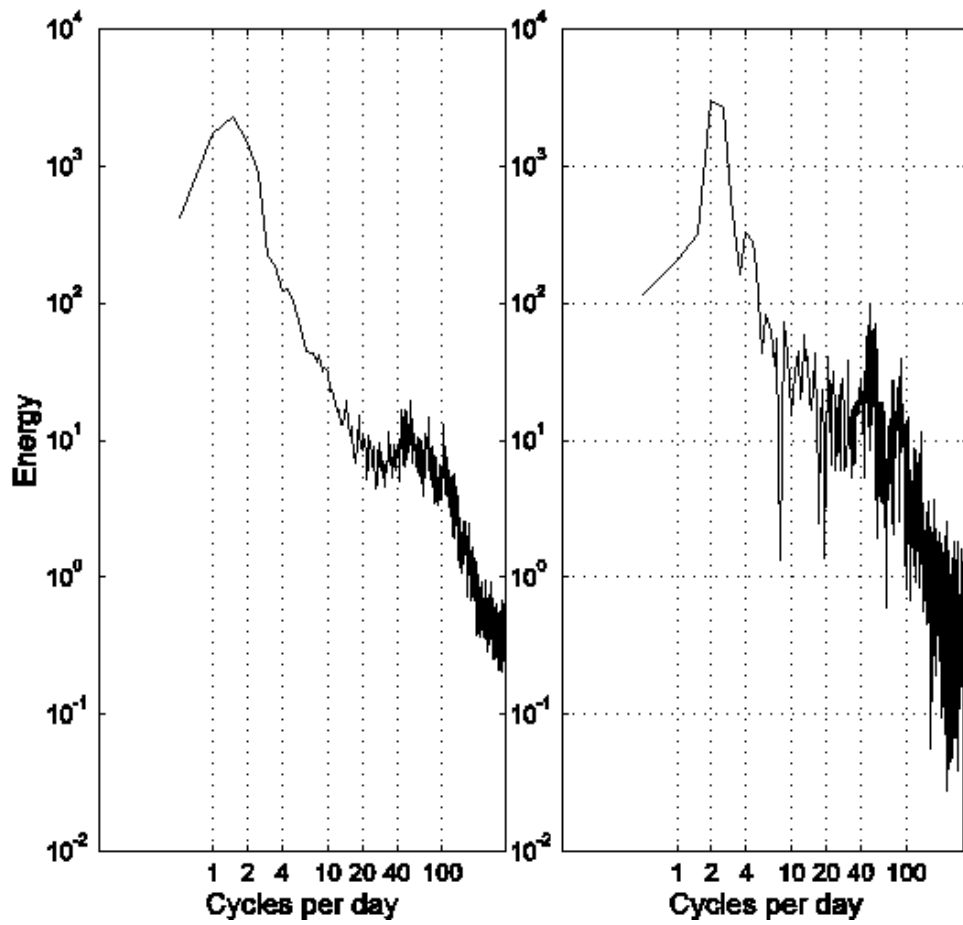
Fig. 1211. Energy spectra of the first internal mode at the CMO mooring for the period day 210 – 245 (left), and the period 241 – 245 (right).

5
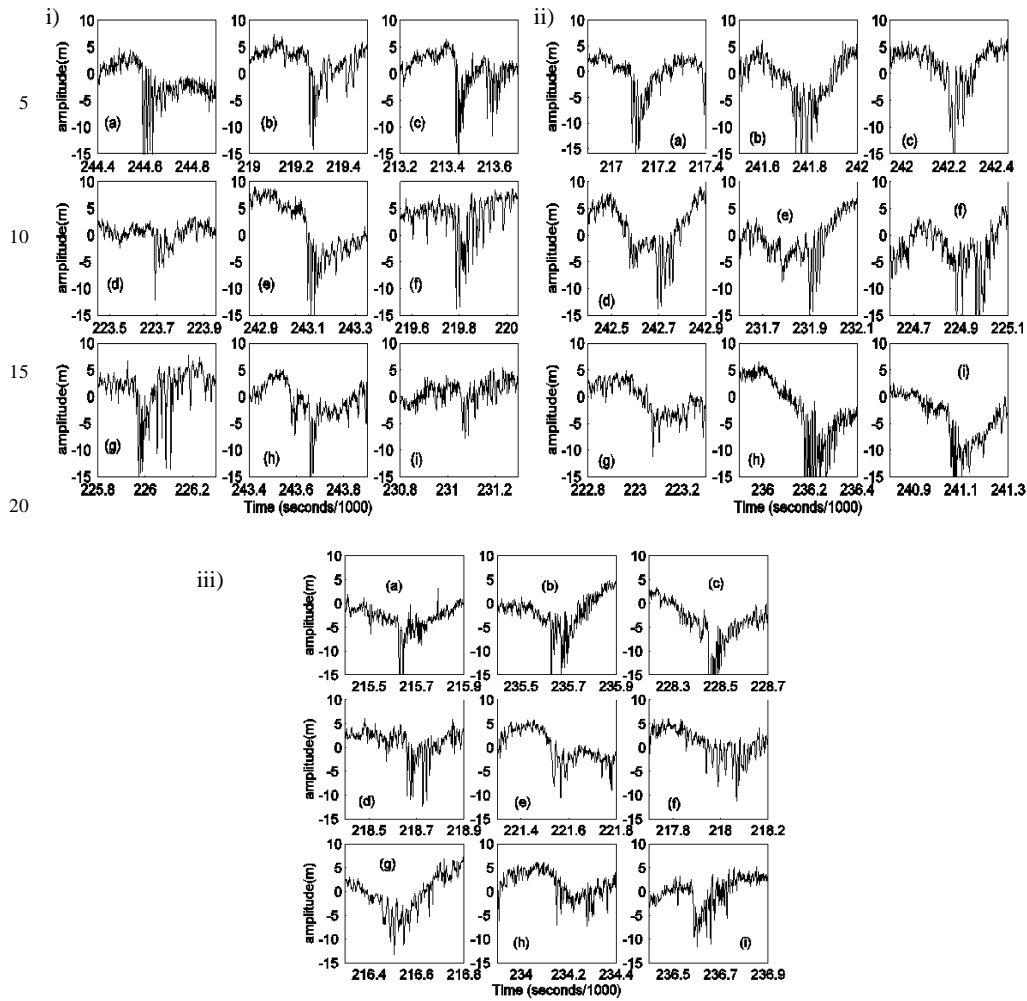
Fig. 1312. Observations at the CMO Mooring site over a semi-diurnal period. Top left, i), sections of
the record similar to events observed over a tidal period in the model runs of Fig. 10 iii). Top right, ii),
same as i) except the record is a little bit more complicated over a tidal period. Bottom, iii), same as ii).

44
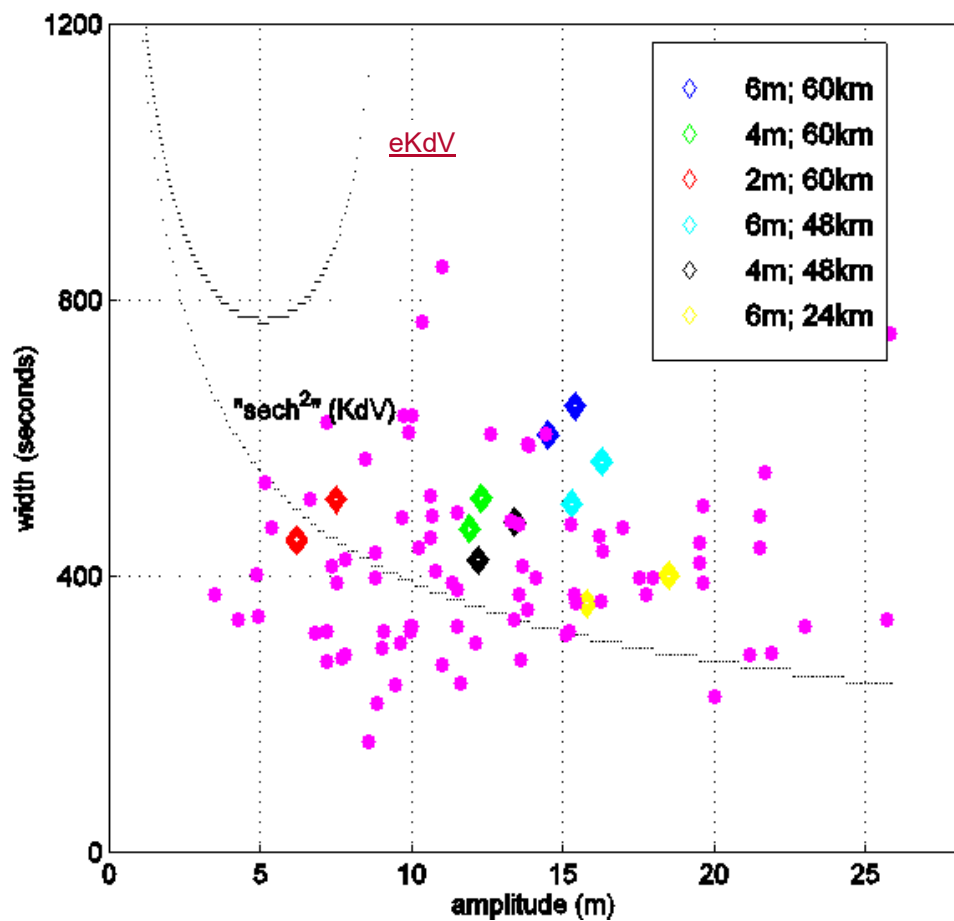
Fig. 1413. Wave amplitude vs. wave width at the CMO mooring for waves from all events during the period day 210 - 245. Also plotted are the two leading waves from six of the nine model runs shown in Fig. 10 (diamonds).

5

Supplementary Figure

Fig. S1. Quadratic nonlinear parameter, α, divided by the cubic nonlinear parameter, α_1, as a function of the depth of the upper layer, h_1, and lower layer, h_2. Values for sloping bottom (Cases A and B) and realistic slope and stratification at the CMO site are shown by the broken lines.

Dear John,

You will see that I have responded to all the Reviewers' comments, below, and edited the manuscript accordingly. A marked up version is also included (separate file).

Thanks and best wishes,

Kieran O'Driscoll

Response to Referee #1 comment
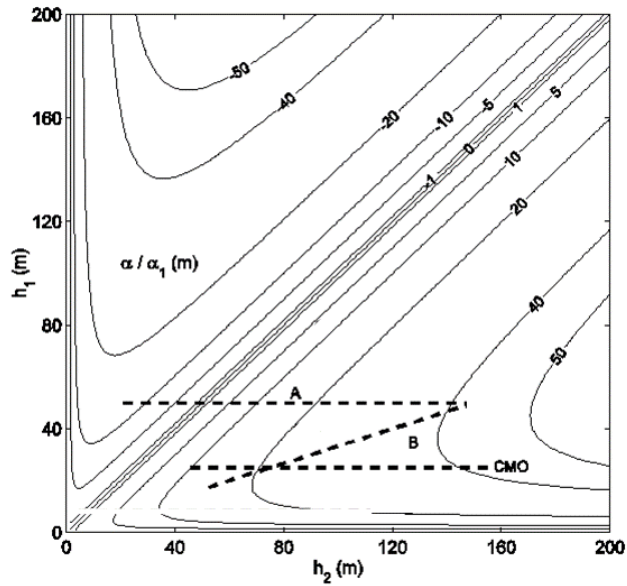
Kieran O'Driscoll thanks the reviewer for their 2nd review.

Review of "Simulations and observation of nonlinear waves on the continental shelf: KdV solutions" (revised) by Kieran O'Driscoll and Murray Levine The paper has been significantly revised and greatly improved. I do not have any further major comments. But I can point the authors to a recent paper by Grimshaw and Yuan (2016) in Physica D volume 333, pp 200-207, who also integrated the KdV equation for propagation of undular bores up a slope. In particular that paper provides an explanation for the effect of a critical point of polarity change on an undular bore, as seen in the authors figure 1, panels 100, 110, 130 km, where after the critical point, one sees a depression rarefaction wave with elevation solitary waves riding on it. This leads to the lack of rank-ordering, and can be contrasted with their figure 3 where there is no polarity change, but is comparable with figure 4 where there is a polarity change.

Response: The following sentences have been included in relation to this feature (last paragraph of 2.1.1):

These leading nonlinear waves mature into rank ordered solitary waves by $65 km$, a feature observed out to $95 km$. Grimshaw & Yuan (2016) have recently shown that the rank ordering is retained in shoaling waters as long as the waves do not encounter a critical point of polarity change on the waves of depression, i.e. $\alpha < 0$ always. This was not the case for Case A (above, Fig. 1, and CMO, below, Fig. 4).

Response to Referee # 2 comments

Kieran O'Driscoll thanks the reviewer for their substantial 2nd review. I have reworked the paper to include all the reviewer's comments, see below.

The author's justification for not considering rotational effects is not correct and is inadequate. A two-dimensional model just means the fields are functions of two spatial variables, say x and z. There can still be flow in the third (lateral) direction. It is well known that rotation does affect internal solitary waves on time scales of the order of an inertial period. In particular energy is radiated behind the internal solitary wave in the form of long inertia-gravity waves. Given enough time the leading ISW can disappear and the trailing IG waves can steepen and form new ISWs. See, for example, Grimshaw et al (2014) or Lamb & Warn-Varnas (2015). In addition, rotation can inhibit an internal tide from steepening and forming ISWs (e.g., Helfrich & Grimshaw 2008). So this begs the question of why the effects of rotation were not considered when making comparisons with the CMO data. Why isn't the Ostrovsky equation being used? As a previous reviewer pointed out, refering to large amplitude ISW solutions of the eKdV equation as "tanh" waves is not recommended. There is an analytical expression for these waves in terms of tanh functions however the waves only look like a tanh function when they are very long with a flat-crest and none of the waves in this paper are remotely close to this shape. For this reason an alternative form of the solitary wave solutions, written in terms of a sech function, is usually used. I think the paper needs considerable revision. The shoaling case with the sloping pycnocline is interesting and the comparisons with CMO observations is a useful addition to the literature however rotational effects should be included or a justification for not including them should be provided. An estimate could be made of the distance over which rotation would affect the waves.

Thanks. *Grimshaw & Helfrich (2014) and Alias, Grimshaw & Khusnutdinova (2014) state that rotation effects become important after several inertial periods. For the 3 cases presented, Cases A, B and CMO, values of c are shown as the waves propagate shoreward in Figs. 1a, 3a 4a, respectively.*

For Case A, for the first 100km of travel, solitary wave speed is estimated at

$$V = c + \frac{\alpha\eta_0}{3}$$ *=0.7m/s. Given an inertial period of 18.67 hrs at 40N, the waves will travel about 95km in 2 inertial periods and into 130 km in a third.*

For Case B, the waves will propagate the 95km considered in about 2 inertial periods.

For the CMO case, the waves are a bit slower and so rotation may become important beyond ~100km of travel. However, the discussion of results of KdV versus eKdV models (section 2.2) is mostly concerned with model runs to 60km (e.g. Fig. 6), as is the discussion comparing model results to observations (Figs. 9-13).

We did not include rotation in our model since it is based on the work and model of Holloway et al. (1997) who explicitly ignored rotation. Part of the reason we conducted this work was to compare model result waves with both theoretical solitons and waves observed waves at the CMO. And it has been discussed that exact solitary waves do not exist in the ocean due to effects of rotation, viscosity, etc., see e.g. Lamb & Xiao (2014).

All references to 'tanh' waves have been removed except in one instance, where the term 'table-top' is introduced and reads as follows p13, line 18:

Solitary type solutions to the KdV ($sech^2$) and to the eKdV ('table-top' waves with tanh type solutions, see e.g. O'Driscoll 1999 and references within) are fitted to the leading waves (Fig. 6d-e).

Comments

1. Page 4, line 1. This sentence implies that the nonlinear terms are not important before the waves shoal which is not true

Agreed, done. Thanks. Sentence has been changed to the following:

As the internal tide shoals, the nonlinear terms in the Navier-Stokes equations can cause these tidal waves of finite amplitude to evolve into packets of high frequency nonlinear waves.

2. Page 4, line 16: "For the model cases ....." makes no sence

Thanks, done. New sentence reads

Whereas most modelling studies regarding wave propagation over linear bottom sloping realistic topography have focused on the behaviour of a single soliton, this work is concerned with the development and evolution of a packet of solitary waves.

3. Page 5 equations 1 and 2. These equations don't fit in the sentence properly. Also, I suggest just giving the eKdV equation and saying that when α1 = 0 the equation reduced to the KdV equation.

Done. This now reads

All cases have been run within the quadratic nonlinear framework of the KdV equation, and the results are compared with an extended form of it, the eKdV Eq.(1) model, written as

$$\eta_t + c\eta_x + (\alpha + \alpha_1\eta)\eta\eta_x + \beta\eta_{xxx} = 0 \qquad\qquad 1$$

which reduces to the KdV equation when $\alpha_1 = 0$.

For the KdV and eKdV equations to be valid, the leading two terms must constitute the primary balance ….

4. Page 5, lines 20–21: "Nonlinear transformation of the internal tide leads to the generation of nonlinear waves". This doesn't make sense. You are saying a

nonlinear wave leads to the generation of nonlinear waves. You mean something like "Nonlinear steepening of the internal tide leads to the generation of a packet of short nonlinear waves which ...". On a similar vein, on page 8, lines 9 it is stated that 'the internal tide steepens and rapidly becomes nonlinear'. The internal tide is nonlinear from the start — otherwise it wouldn't be steepening! Following this what is meant by "the internal tide becomes more nonlinear"? What is the measure of the nonlinearity?

Thanks. Done. These sentences now read

Nonlinear steepening of the internal tide leads to the generation of a packet of short nonlinear waves which tend to become solitary-like in form as the dispersive term becomes important. (p5, lines 19-21)

p8. Yes, thanks. The input at the open boundary (sine wave) is linear but the system (model) is non-linear, so steepens as soon as it enters the model domain. The steepening is a measure of the nonlinearity, governed by the KdV/eKdV systems. So the sentence now reads

The internal tide steepens from a sinusoid at the open boundary, rapidly becoming nonlinear, resulting in the generation of a shock-like front and subsequent undulations by $l \approx 50 km$. (p8, lines 10-12)

5. Page 6, lines 19–20. This sentence is not very clear. Perhaps "... we investigate two cases with a constant sloping bottom, one with a horizontal interface and one with a sloping interface, ..."

Thanks. Done.

6. Page 7. Equation (4). Here a shoaling term that is not present in equations (1) and (2) is included. The first two equations should include the shoaling term. The shoaling term is not ever mentioned. I also suggest giving expressions for the nonlinear and dispersive parameters to readers can see, for example, how α changes sign, α1 6= 0 and that β > 0.

Thanks, done, as follows

The term in Q accounts for the horizontal variability of the ocean (see, e.g., Zhou & Grimshaw (1989), Pelinovsky et al. (1977) and Holloway et al. (1997)) and is given by

$Q = \dfrac{Mc^3}{M_0 c_0{}^3}$ with $M = \dfrac{h_1 + h_2}{h_1 h_2}$ where h_1 and h_2 are upper and lower layer thicknesses,

respectively. The coefficients of the KdV and eKdV equations are greatly simplified for a

two-layer fluid and are written (e.g. Ostrovsky & Stepanyants, 1989) $c = \sqrt{\dfrac{g\Delta\rho}{\rho} \dfrac{h_1 h_2}{h_1 + h_2}}$;

$$\alpha = \frac{3}{2} c \frac{h_1 - h_2}{h_1 h_2} ; \qquad \beta = c \frac{h_1 h_2}{6} ; \qquad \alpha_1 = -\frac{3c}{8 h_1{}^2 h_2{}^2} \left(h_1{}^2 + h_2{}^2 + 6 h_1 h_2 \right).$$

7. Page 7. Please mention the numerical method used to solve the equations.

Done, reads:

We employ the same finite difference scheme as Holloway et al. (1997) to solve the eKdV equation Eq.(3) numerically. The finite difference scheme is a central difference method, (e.g. Lapidus & Pinder, 1982), which was first developed for the KdV equation by Berezin (1987), and for the variable coefficients KdV by Pelinovsky et al. (1994). See O'Driscoll (1999) for further details. (top p.8)

8. Page 7 line 15: "We chose the starting layer thicknesses at l = 0 to be ... with a bottom ...'

Done

9. Page 7, line 18: " ... at a water depth ..."

Done.

10. Page 9, line 3: Please define what is meant by the leading face? Since the internal tide is sinuosoidal this is ambiguous. Do you mean the front of the crest or the front of the trough?

Done, thanks.

the front of the wave trough

11. Page 9, line 6: Do you mean the slope decreases rapidly? Above you say the leading face steepens but the steepening slows down, then you say the rate of change of the slope changes sign? I find this confusing.

Yes, thanks, done. I have just changed it to the slope decreases rapidly.

12. Page 9, line 7. Where is the second shock-like front?

Sentence removed.

13. Page 9, lines 10–13. I don't see what the difference in the magnitudes of the nonlinear and dispersive terms has to do with the phase speed of the waves. Aren't waves propagating with phase speed less than c simply because they are in the wave trough where $\eta < 0$?

No. Solitary waves always travel faster than gravity waves, $V = c + \dfrac{\alpha \eta_0}{3}$.

Given $\alpha = \dfrac{3}{2} c \dfrac{h_1 - h_2}{h_1 h_2}$ (these 2 expressions were included in the original version, see discussion paper), it is seen *α>0 when* $h_2 > h_1$, thus, for waves of depression, $\eta_0 < 0$, so that $\alpha\eta_0 > 0$, and *V>c.* The same argument is made for solitary waves of depression.

In the following paragraph mention of the wave alternating between being more nonlinear and dispersive is made. This does not make sense to me and this whole paragraph seems unhelpful. The nonlinear and dispersive terms vary across a given wave, changing sign at different locations in some instances. It does not seem helpful to say that at one value of x where $\eta xxx = 0$ and $\eta\eta x \neq 0$ the wave is more nonlinear than dispersive. The wave should be viewed as a whole. I recommend removing this whole discussion along with Figures 2(a) and 4 and accompanying discussion.

Done. I removed reference to Fig 2b and Fig 5 and the associated lines.

14. Page 10, lines 5: The KdV or eKdV equation are not subject to KelvinHelmholtz instabilities.

Sentence removed.

15. Page 11, line 10: what is the 'back-face' of the wave? The back of the crest or the back of the trough?

Thanks. Same as 10 above: on the front of the internal tide wave trough

16. Page 11, lines 12–13. "the number of solitary-like waves seems to have been reduced to the leading two waves". On what basis were some waves judged to be solitary-like and other waves not?

From Figs. 4b and c. Solitary waves travel faster than regular gravity waves:

$V = c + \dfrac{\alpha\eta_0}{3}$ (e.g. O'Driscoll 1999), included in original version (see OSD manuscript). So, the troughs of solitary waves (blue) travel to the left, Fig. 4c. Only the first two travel to the left after 80km.

17. Page 11, lines 19–20: The instability must have something to do with the numerical scheme. The dispersion parameter may get small. It is never 0

Agreed. The sentence has been changed to the following:

The internal tide becomes numerically unstable beyond $l = 130 km$.

18. Page 12, lines 4. Here χ is defined. If use of χ is retained it should be defined when first used

Done. All reference to χ has been removed, see 13 above.

19. It would be useful to plot values of α1 when solutions of the eKdV equation are being discussed.

Sorry, this was included in the previous manuscript, Fig. S1, I forgot to reference it. Thanks.

20. Page 19, line 9: When you say 'using CMO site parameters' are you using a continuous stratification? How do the parameters for the observed (i.e., continuous)

stratification compare with those for the two-layer approximation? I am not convinced that a two-layer approximation is appropriate even if they waves are mode-one. A figure showing the observed stratification should be provided and justification for the choice h1 = 25 m should be given.

A 2-layer stratification was used, which was a realistic model given conditions at the CMO site in August 1996, and was chosen following discussed with my advisor, Murray Levine. Examples of the stratification at the CMO site are given in Boyd, T., Levine, M.D., and Gard, S.R.: Mooring observations from the Mid-Atlantic Bight, Oregon State University, Data Report 97-2, pp. 226, 1997 (referenced in text). Also, please see below a section across the site of the CMO shelf, shows an upper mixed layer of ~25m separated from a very weakly stratified pycnocline (from Barth et al. 1998, referenced).
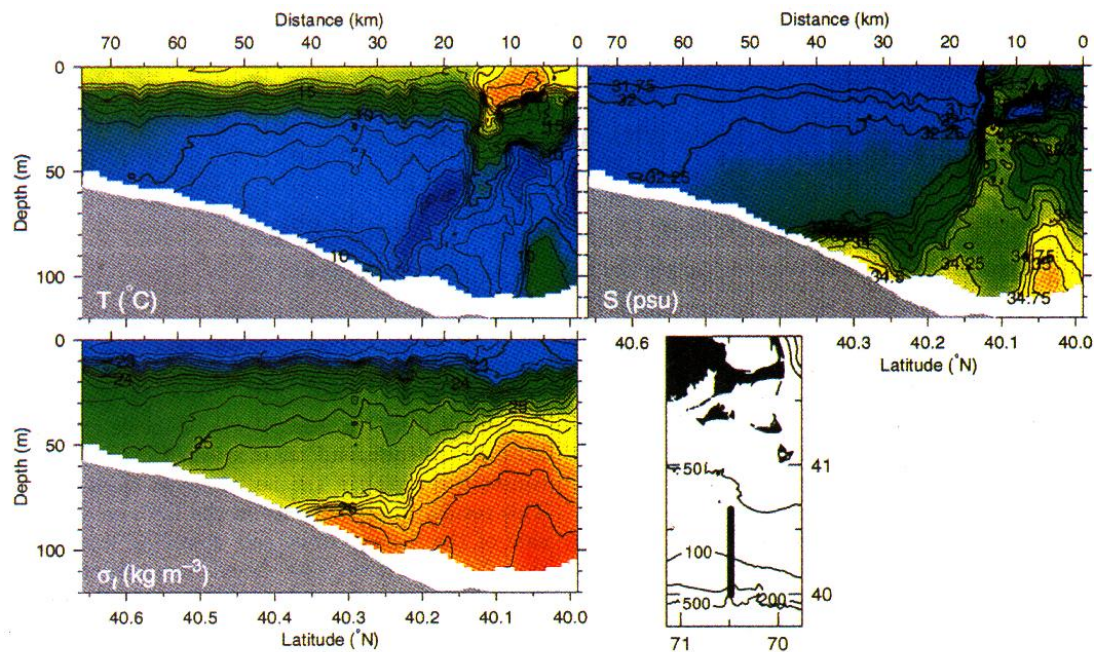
Figure 1. Cross-shelf sections of temperature, salinity and density along 70.48°W from 13:01 to 19:35 UTC on August 21, 1996. Gridded data locations are shown as light dots. The location of the cross-shelf section is indicated by a thick line on the map.

21. Figures: The figures should be improved. For example in Figure 1(a) the ticks along the x-axis should be the same in all panels like they are in figure 2(a) (and I think ticks at 20 km intervals is better than at 30 km intervals). Many figures are of poor quality but perhaps I got low resolution versions of them? In Figure 7 it is hard to distinguish the two curves in the upper left panel. In this figure intervals of 11 along the bottom axis is odd. How about going by 10?

Thanks. Tick marks are the same for all panels Fig. 1, 3, 4.

The close up in Fig 7b is a close up of 7a (now Fig. 6).

We used 44000s as the semi-diurnal period, so 11000s is ¼ of the period, etc.